AD-A104 344 AIR FORCE WRIGHT AERONAUTICAL LABS WRIGHT-PATTERSON AFB OH F/G 20/5
MASS SPECTROMETRY OF THE CO2 LASER PLASMA.(U)
JUN 81 D E TOODLE
UNCLASSIFIED AFWAL-TR-80-2029 NL

1 of 1
AD
A104344

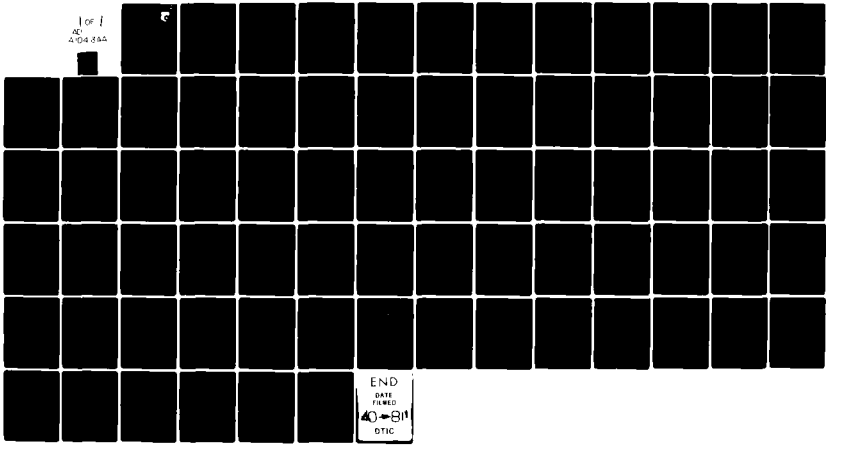

END
DATE FILMED
10-81
DTIC

AFWAL-TR-80-2029

MASS SPECTROMETRY OF THE CO_2 LASER PLASMA

David E. Toodle

June 1981

Final Report for Period July 1975 - September 1979

Approved for public release; distribution unlimited.

AERO PROPULSION LABORATORY
AIR FORCE WRIGHT AERONAUTICAL LABORATORIES
AIR FORCE SYSTEMS COMMAND
WRIGHT PATTERSON AIR FORCE BASE, OHIO 45433

NOTICE

When Government drawings, specifications, or other data are used for any purpose other than in connection with a definitely related Government procurement operation, the United States Government thereby incurs no responsibility nor any obligation whatsoever; and the fact that the government may have formulated, furnished, or in any way supplied the said drawings, specifications, or other data, is not to be regarded by implication or otherwise as in any manner licensing the holder or any other person or corporation, or conveying any rights or permission to manufacture use, or sell any patented invention that may in any way be related thereto.

This report has been reviewed by the Office of Public Affairs (ASD/PA) and is releasable to the National Technical Information Service (NTIS). At NTIS, it will be available to the general public, including foreign nations.

This technical report has been reviewed and is approved for publication.

David E. Toodle

David E. Toodle, Captain, USAF
Project Engineer

Donald P. Mortel

DONALD P. MORTEL
Act'g Branch Chief,
Energy Conversion Branch

FOR THE COMMANDER

D. David Randolph

MAJOR D. DAVID RANDOLPH
Act'g Chief, Aerospace Power Division
Aero Propulsion Laboratory

"If your address has changed, if you wish to be removed from our mailing list, or if the addressee is no longer employed by your organization please notify AFWAL/POOC *, W-PAFB, OH 45433 to help us maintain a current mailing list".*

Copies of this report should not be returned unless return is required by security considerations, contractual obligations, or notice on a specific document.

SECURITY CLASSIFICATION OF THIS PAGE (When Data Entered)

REPORT DOCUMENTATION PAGE

READ INSTRUCTIONS BEFORE COMPLETING FORM

1. REPORT NUMBER: AFWAL-TR-80-2029	2. GOVT ACCESSION NO.: AD-A104344
3. RECIPIENT'S CATALOG NUMBER:	
4. TITLE (and Subtitle): MASS SPECTROMETRY OF THE CO_2 LASER PLASMA	5. TYPE OF REPORT & PERIOD COVERED: Final, July 1975 – September 1979
	6. PERFORMING ORG. REPORT NUMBER:
7. AUTHOR(s): David E. Toodle, Capt., USAF	8. CONTRACT OR GRANT NUMBER(s):
9. PERFORMING ORGANIZATION NAME AND ADDRESS: Aero Propulsion Laboratory (AFWAL/POOC), Air Force Wright Aeronautical Laboratories (AFSC), Wright-Patterson Air Force Base, Ohio 45433	10. PROGRAM ELEMENT, PROJECT, TASK AREA & WORK UNIT NUMBERS: 61102F/2301/S2/13
11. CONTROLLING OFFICE NAME AND ADDRESS: Aero Propulsion Laboratory (AFWAL/POO), Air Force Wright Aeronautical Laboratories (AFSC), Wright-Patterson Air Force Base, Ohio 45433	12. REPORT DATE: June 1981 13. NUMBER OF PAGES: 68
14. MONITORING AGENCY NAME & ADDRESS (if different from Controlling Office)	15. SECURITY CLASS. (of this report): Unclassified 15a. DECLASSIFICATION DOWNGRADING SCHEDULE

16. DISTRIBUTION STATEMENT (of this Report)

Approved for public release; distribution unlimited.

17. DISTRIBUTION STATEMENT (of the abstract entered in Block 20, if different from Report)

18. SUPPLEMENTARY NOTES

19. KEY WORDS (Continue on reverse side if necessary and identify by block number)

CO_2 Lasers
Mass Spectrometry
Plasma Chemistry
Discharge Electrochemistry
Glow Discharges
Electric-Discharge Lasers

20. ABSTRACT (Continue on reverse side if necessary and identify by block number)

The neutral and ion chemistry of the CO_2 laser mixture have been studied in detail by using a quadrupole mass spectrometer and a theoretical model. Experimentally, CO_2 is observed to dissociate primarily by direct electron impact producing the dominant neutral species CO and O_2. Little or no N_2 dissociation occurs in a N_2/Ar discharge; however, the dissociation of N_2 increases when it is added to a mixture containing CO_2. Consequently, the dominant nitrogen oxide in discharges containing CO_2 and N_2 is NO. The major positive ions are CO_2^+, O_2^+, CO^+, N_2^+; and the major negative ions are NO_2^-, NO_3^-, O_2^-, O^-, CO_3^-.

DD FORM 1 JAN 73 1473 EDITION OF 1 NOV 65 IS OBSOLETE

SECURITY CLASSIFICATION OF THIS PAGE (When Data Entered)

BLOCK 20 (Continued)

CO_2 dissociation is reduced by as much as 20% at a discharge current of 80mA with the addition of 2% H_2. Techniques for using a mass spectrometer to sample from glow discharges are also discussed.

FOREWORD

This work was performed at the plasma physics laboratory in the Aero Propulsion Directorate of the Air Force Wright Aeronautical Laboratories under in-house project 2301S213. The project monitors were J.F. Prince and D.E. Toodle in succession.

There were many investigators of this research, and their contributions are gratefully acknowledged and identified in this report. The author wishes to thank A. Garscadden and P. Bletzinger for their review of the draft, and M. Matosky for his sketches of the experimental apparatus.

TABLE OF CONTENTS

LIST OF ILLUSTRATIONS

SECTION I

INTRODUCTION

The requirements for mass spectrometric analysis of gas samples are well known and have been described in detail (Reference 1). Analysis of glow discharges in molecular gases or gas mixtures is more difficult because of composition change due to electrochemical activity. One example is that of the sealed-off carbon dioxide laser which is the subject of this report. Mass spectrometric measurement of steady-state component concentration in the CO_2 laser discharge has been shown to be feasible (Reference 2). Measurement of reaction rates and transient concentration is also possible (Reference 3). The evidence indicates that valuable information concerning the plasma chemistry of the discharge can be obtained with the aid of a mass spectrometer (References 3-22).

The dissociation of CO_2 is a major problem in sealed-off CO_2 lasers. The carbon monoxide formed competes with the CO_2 for vibrational excitation; and the atomic and molecular oxygen formed affects the stability of the discharge (Reference 14). Dissociative attachment:

$$CO_2 + e^- \rightarrow CO + O^- \qquad (1)$$

and collisional dissociation:

$$CO_2 + e^- \rightarrow CO + O + e^- \qquad (2)$$

both contribute to the dissociation process (References 5 and 8). The dissociation of CO_2 seems to obey the general reaction

$$CO_2 \rightleftharpoons CO + 1/2\ O_2 \qquad (3)$$

with an equilibrium constant that varies with the diameter of the tube (Reference 9) and at pressures less than 0.5 torr (Reference 6). The

dissociation coefficient, which is defined as $\frac{\alpha}{p}$ where α is the number of dissociations occuring per electron per cm of path length and p is the gas pressure, also increases with reduced field strength (E/p) (Reference 7).

CO_2 dissociation can be reduced by the addition of H_2 to the discharge (References 10 and 11). The H_2 acts as a catalyst to reform the CO_2, and the equilibrium constant for reaction (Equation 3) is found to be linearly dependent on the H_2 concentration (Reference 5).

The major neutral contaminants in a $CO_2/N_2/He$ discharge appears to be CO, O_2, NO, N_2O, and NO_2 (References 3 and 4). CO and O_2 concentrations are comparable to the concentrations of the initial fill gases $CO_2/N_2/He$, and the nitrogen oxides are in concentrations less than 1%. Although the concentrations of the nitrogen oxides are small, the laser gain is affected by them (Reference 12).

Positive ions have also been identified (References 16 and 17) as well as positive cluster ions (Reference 18). It is generally agreed among the investigators that CO_2^+ and O_2^+ are the most dominant positive ions formed. Since the positive ions are not known to affect the discharge, the importance of negative ions and negative ion chemistry is apparent.

Exhaustive studies have been done on the identification of contaminants in a $CO_2/N_2/He$ discharge as evident from the above. The only exception, at the start of this project, was the identification of the negative ion species. Hence, this identification was accomplished first (References 14 and 15). A more complete investigation of the effects of hydrogen in a CO_2/N_2 discharge was also accomplished under this project (Reference 19).

The major contaminant species CO and O_2 were tracked over a wide range of current values as well as the CO_2 concentration. This experimental data was compared with a chemistry code (Reference 20) in order

to identify the most important reactions that form the contaminant species. The above comparison, known as the plasma synthesis approach (Reference 21) was the last investigation accomplished under this project (Reference 22).

The plasma synthesis approach initially involves the analysis of a single gas component. This analysis includes a comparison of the experimental results with the code calculations. Next, an additional component is added and the analysis is repeated on the resultant mixture. This procedure of adding components and then analyzing the resultant mixture is repeated until the total laser mixture is synthesized. The synthesis approach is very easily implemented and it gives very reliable results as will be shown later.

The ultimate goal of this project was to investigate the plasma chemistry of the CO_2 laser discharge and, thereby, indentifying some of the plasma chemical processes responsible for the production of contaminants. A knowledge of these basic processes may then be used to make closed-cycle CO_2 lasers more attractive to the Air Force. The Air Force is interested in closed-cycle lasers not only for their compactness, but also because they allow the use of isotopic CO_2 gas. The compactness results from the elimination of large storage tanks, and the use of isotopic CO_2 offers the choice of wavelength selection corresponding to a particular atmospheric transmission window. Since this project was the first of its kind for this laboratory, experimental techniques have also been included, hence, rendering this report a guide in any future research in this area.

SECTION II

EXPERIMENTAL ARRANGEMENT AND PROCEDURE

Figure 1 is a schematic diagram of the experimental arrangement. The gases used were of research grade with a minimum purity of 99.998%. Among the pure gases used were Ar, He, CO_2, N_2, and H_2. The gas mixture used was 1.98% H_2/25.3% CO_2/ 72.72% N_2. The mixing manifold (E in Figure 1) normally contains glass beads in order to aid in a thorough mixing of the gas components. The individual gas flow rates were measured by Hastings mass flowmeters. The pressure transducers, used in conjunction with the flowmeters, are represented by A, B, C and D in Figure 1. The flow rates were accurate to $\pm$ 1% for the rare gases and those of the molecular gases were accurate to $\pm$ 5%.

Several types of discharge tubes, each with the sampling orifice in a different location, were used in the experiments. The one shown as G in Figure 1 has the sampling orifice (H) on the side of the tube located in the middle of the two electrodes. The tube was constructed of quartz with a double-wall. The outer jacket was used for cooling water. The inner diameter of the tube was 2.50cm, and the hollow electrodes were separated by a distance of 30cm. The electrodes were made of Kovar and the cathode was located upstream of the gas flow. Pressure measurements were made behind the cathode by a differential capacitance manometer (L) manufactured by MKS Instruments, Inc., and the cryosorption pump (M) was used to pump out the reference port of the manometer.

The partial pressure of a particular gas component in the discharge tube is given by

$$p_s = p \frac{Hs}{H} \tag{3}$$

where p_s is the partial pressure, p is the total pressure, H_s is the flow rate of the gas component, and H is the total flow rate. The total

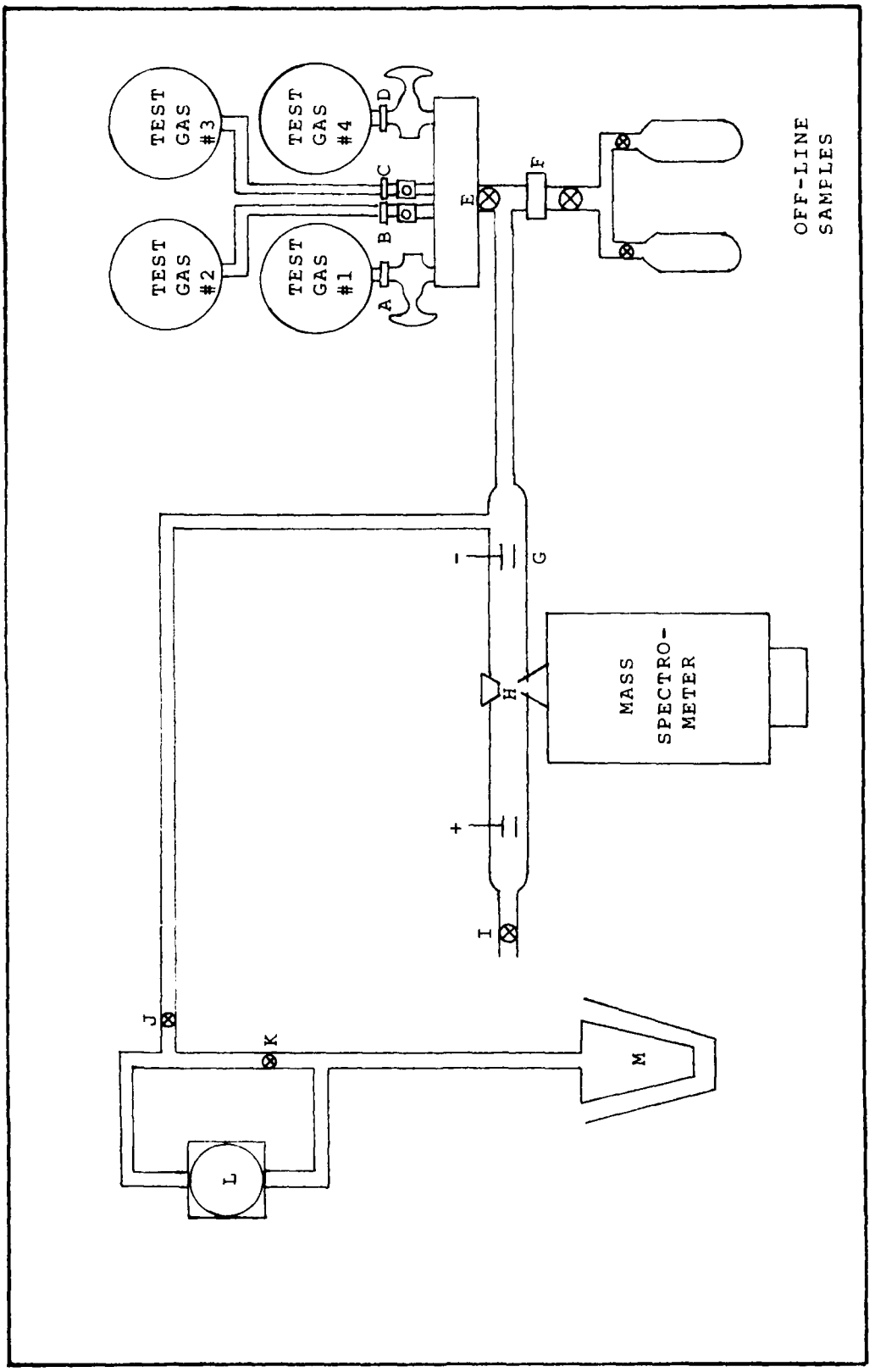

Figure 1. Experimental Arrangement of an On/Off-Line Mass Analyzer System

flow rate, usually given in standard cubic centimeters per minute (SCCM), is just the sum of the flow rates of the individual gas components:

$$H = \sum_s H_s \tag{4}$$

The gas residence time, which is the length of time that a portion of gas is in the discharge before it is sampled by the spectrometer, is given by

$$\tau = \frac{A \ell p}{H p_o} \tag{5}$$

where A is the cross sectional area of the discharge tube, p_o is standard atmospheric pressure, and ℓ is the length from the cathode to the sampling orifice. Complete derivations of Equations 3, 4, and 5 are given in Appendix A.

A quadrupole mass spectrometer, manufactured by Extranuclear Laboratories, Inc., was used to sample the discharge. The spectrometer contains two differential pumping stages (see Figure 2). The first stage is pumped with a turbomolecular pump and the second stage is pumped with a diffusion pump. Both pumps are backed by a forepump. In normal operation of the spectrometer, the pressure in both chambers are monitored with ion gauges; however, during the pump down phase, the pressure can be monitored with thermocouple gauges. The lowest pressures that were attainable in this experiment were $\sim 10^{-6}$ and $\sim 10^{-7}$ torr in the front and rear chambers, respectively.

The ion gauge in the rear chamber is connected to an interlock system so that the high voltages to the mass filter and particle multiplier, both of which are in the rear chamber, are automatically shut off if there is a partial loss in vacuum. The upper limit of the pressure is pre-selected, and this limit is usually set at 10^{-6} torr. For example, if the pressure in the rear chamber exceeds 10^{-6} torr, the high voltages are automatically shut off. The purpose of

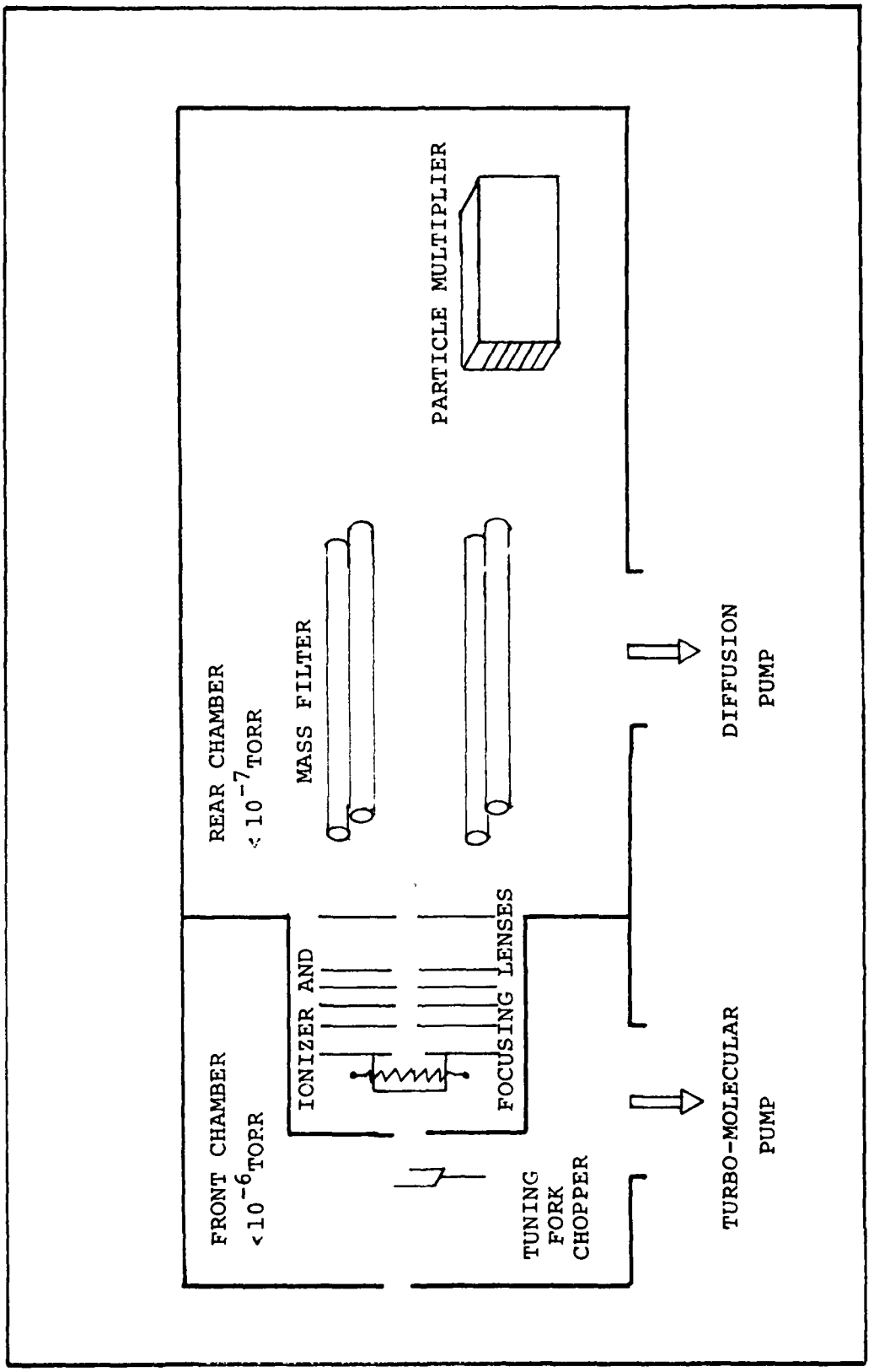

Figure 2. Cross Sectional View of the Quadrupole Mass Spectrometer

this interlock system is to prevent damaging arcs from occurring inside the mass filter and particle multiplier assemblies. Because of the differential pumping scheme, the pressure in the front chamber can be as high as 10^{-4} torr without affecting the operation of the mass filter and multiplier in the rear chamber.

Neutral species were sampled from the positive column, while positive and negative ions were sampled from the afterglow behind the cathode and anode, respectively. The samples entered the spectrometer as molecular beams produced by the molecules effusing through the sampling orifice. The type of flow from the orifice can either be one of two extremes: molecular flow or free jet expansion. The type of flow also depends on the size of the orifice and the pressure within the discharge tube. The advantages and disadvantages of each type of flow regime will be discussed in the following two paragraphs.

In the molecular flow regime, molecular species s flows through the orifice at a rate given by

$$\psi_s = 1/4\ n_s\ \bar{v}_s\ A \qquad (6)$$

where n_s is the steady state number density within the discharge tube, $\bar{v}_s$ is the average molecular speed, and A is the area of the orifice. Molecular flow through an orifice can be achieved at a pressure where the mean free path of molecules is between 15 and 40 times the diameter of the orifice (Reference 1). The advantages of molecular flow (also called effusive flow) is that the molecules travel approximately independent of each other, thereby minimizing chemical reactions that might occur within the beam. This aspect of molecular flow would ensure that the chemical constitutes of the sample are the same as those in the discharge tube. The intensity of the beam falls off as $1/r^2$ and is proportional to cos (θ), where r is the distance from the orifice to any point on the axis of the spectrometer and θ is the angle from the axis of the beam (Reference 1). Therefore, the orifice must be precisely aligned with the axis of the ionizer in order to obtain a sizeable signal from the mass spectrometer.

The problem of low sensitivity, which is a disadvantage in the molecular flow regime, can be alleviated by a free jet expansion of the molecules through the orifice. This regime occurs when the mean free path is much less than the diameter of the orifice and mass motion of the gas occurs. Also, the gas in a free jet expansion is collision dominated and chemical reactions are highly probable. Therefore, the sample obtained via a free jet expansion does not accurately represent the chemistry of the discharge. This aspect is the major disadvantage of a free jet expansion. A trade-off regime, known as transition flow, occurs when the mean free path is on the order of the diameter of the orifice.

To sample neutrals, the molecular beam is led into an electron impact ionizer. The most common setting of the electron energy is 70eV because the maximum ionization efficiency of a majority of the atomic and molecular gases occur between 60 and 120eV (Reference 23). Another reason is that the energy of the electrons is only approximately mono-energetic; consequently, there is a minimum fluctuation of ion pair production from a fluctuation in the electron energy in the region of maximum efficiency. The disadvantage of the 70eV setting is that other processes such as double ionization, excitation, and dissociation have a high probability of occurring.

The meter reading of the electron energy does not reflect the true energy of the bombarding electrons. This fact is due to the contact potential difference of the electrical connections and space charge effects in the ionizer. The amount of offset is usually a few eV and it depends on the particular construction of the ionizer. The offset can be determined by making appearance potential plots of several known gases. The onset potentials are then compared with the published values of the ionization potentials. The difference is the amount of offset.

Once the ions are formed, they need to be extracted from the ionizer and focused into the mass filter. The ions are extracted by an extractor

lens and the voltage on this lens can be varied from - 20 to + 20 volts. To provide ion focusing, the voltage on each of a series of three lenses can be varied from -400 to +100 volts. The theory of electric mass filtering may be found in Appendix B.

To detect the ions, a 21-stage copper-beryllium particle multiplier is used. The multiplier is positioned off-axis from the mass filter in order to prevent neutrals, photons, and metastables from striking the multiplier. Hence, spurious noise is eliminated, and the signal to noise ratio is greatly improved. The positive ions, therefore, must rely on the high negative potential of the first dynode in order to be deflected toward the multiplier and subsequently detected. The potential of the first dynode is usually kept between -4 and -5kV. When detecting negative ions, however, the polarity of the multiplier must be reversed.

The signal from the particle multiplier is fed into a preamplifier which is a pulse amplifier-discriminator. Counting or current measurements can be made simultaneously or individually on the same signal source. The pulse pair resolution time of the circuit is 0.2 μsec, and the maximum available count rate is 1 MHz. The count rate is placed below the operating frequency of the mass filter so that no stray rf can enter the circuit. Pulse counting is advantageous because noise can be minimized by adjusting the height of the discriminator level.

The signal out of the preamp is then fed into a fast electrometer for further amplification. The detectable current range of this instrument is 2×10^{-11} to 1×10^{-4}A. The signal out of the electrometer is subsequently displayed by an oscilloscope and/or chart recorder.

It is highly desirable to eliminate the background spectrum when interpreting mass spectra. Modulated beam/lock-in amplifier techniques can be used to accomplish this task. A tuning fork chopper with a nominal frequency of 400 Hz is used as the modulator. The chopper physically interrupts the molecular beam in a periodic manner, and the

ions arriving at the particle multiplier have amplitude changes which are at the same frequency as the chopper. The ions and neutrals arriving from the background gas have no such periodic nature. The lock-in amplifier detects these amplitude changes and electronically subtracts the background signal from the total signal, thus, indicating the true signal.

The major experimental variables were the gas pressure, discharge current, and gas residence time. The pressure range of the experiments was from 1 to 32 torr, and the current range was from 5 to 80 mA. In the experiments that used a flowing gas mixture, the gas residence time was adjusted to allow many of the plasma chemical reactions to reach equilibrium. Equilibrium conditions can be determined by noting the concentrations of chemical species as a function of residence time. Since the geometry of the tube is fixed, the residence time for a particular value of the gas pressure can be varied by varying the total flow rate (refer to Equation 5). Figure 3 shows the concentration versus residence time of a few contaminants that are formed in a $CO_2/N_2/H_2$ discharge.

The concentration in the discharge can be predicted with a high degree of accuracy if certain requirements are met. These requirements and the method for determining component concentrations are discussed in Appendix C.

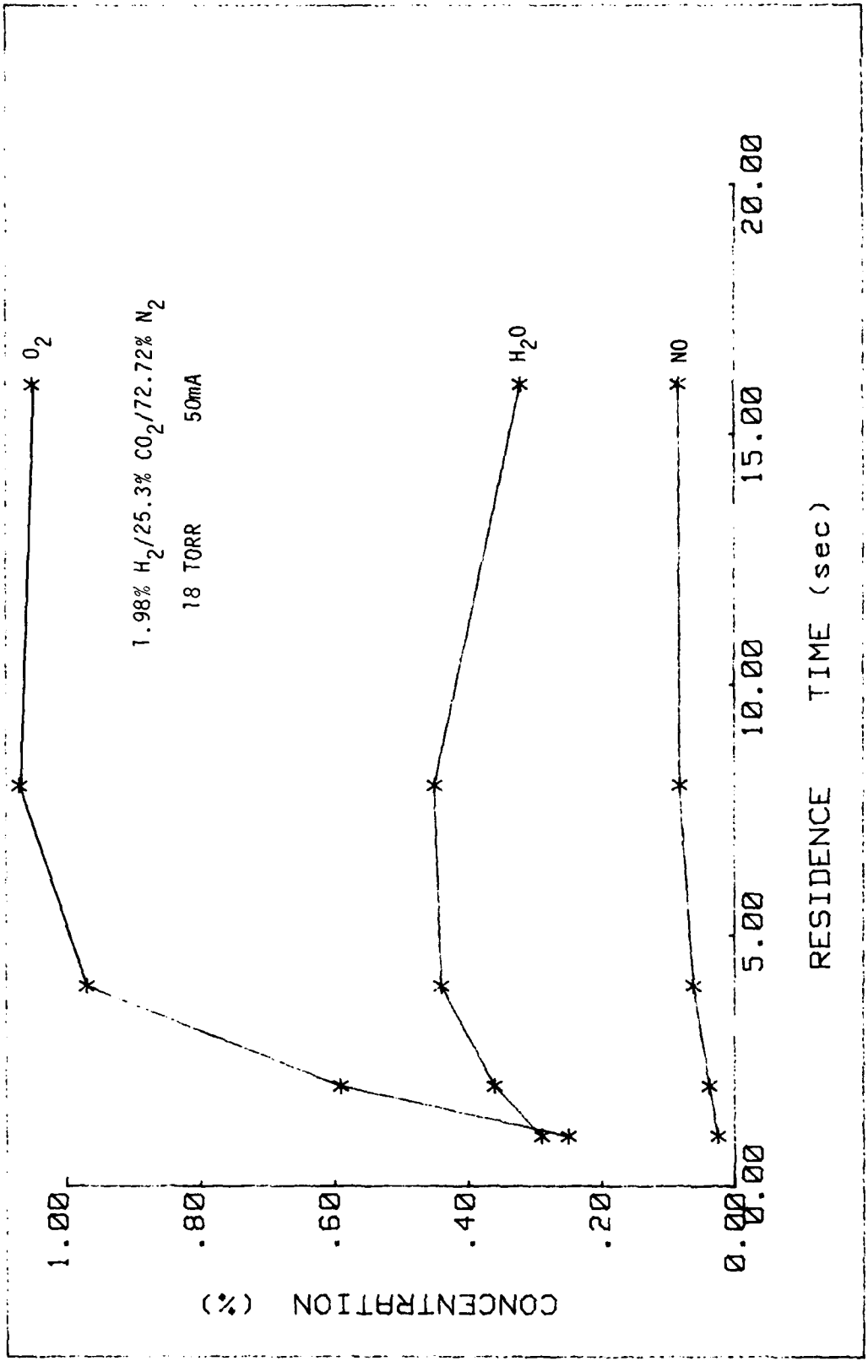

Figure 3. Residence Time Plot (Reference 45)

SECTION III

CHEMICAL MODELING

As a first approach to modeling the neutral chemistry of the discharge, the following simplifications were made:

(1) Nearly all the reactions considered were binary and assumed to be second order and

(2) Only the forward rate constants were considered, while the reverse rate constants were set equal to zero.

Considering mostly second order binary reactions is reasonable since the experiments were carried out at low pressures (2 TORR). The second simplification appears to be extreme; however, the availability of data did not permit the inclusion of reverse rate constants. As will be shown in the next section, these simplifications (along with a few adjustments) resulted in a chemical code that gave fair agreement with the experimental data.

Consider an elementary binary reaction with the following stoichiometry:

$$a_i\ A_i + b_i\ B_i \underset{k_{-i}}{\overset{k_i}{\rightleftarrows}} c_i\ C_i + d_i\ D_i \qquad (7)$$

where k_i and k_{-i} are the forward and reverse rate constants, respectively. The rate of the reaction is given by

$$R_i = -\frac{1}{a_i}\frac{d[A_i]}{dt} = -\frac{1}{b_i}\frac{d[B_i]}{dt} = \frac{1}{c_i}\frac{d[C_i]}{dt} = \frac{1}{d_i}\frac{d[D_i]}{dt} \qquad (8)$$

where the brackets denote number density. Since Equation 7 is assumed to be a second order reaction, the rate of formation of species C_i is proportional to the product of the A_i and B_i number densities, while

the rate of depletion of C_i is proportional to the product of the C_i and D_i number densities. The constants of proportionality are the forward and reverse rate constants, respectively. Therefore, the rate of formation of species C_i is given by

$$\frac{1}{c_i}\frac{d[C_i]}{dt} = k_i [A_i] [B_i] - k_{-i} [C_i] [D_i] = k_i[A_i][B_i] \qquad (9)$$

since $k_{-i} = 0$ by simplification 2. C_i can also be depleted by reacting with other species. For examples, a depleting reaction is given by

$$a_j A_j + c_j C_i \underset{k_{-j}}{\overset{k_j}{\rightleftarrows}} b_j B_j + d_j D_j \qquad (10)$$

where the corresponding rate of depletion is

$$-\frac{1}{c_j}\frac{d[C_i]}{dt} = k_j[A_j][C_i] - k_{-j}[B_j][D_j] = k_j[A_j][C_i] \qquad (11)$$

The net rate of formation of species C_i is determined by summing over all reactions that form and deplete C_i:

$$\frac{d[C]}{dt} = \sum_i c_i k_i [A_i][B_i] - \sum_j c_j k_j [A_j][C_i] \qquad (12)$$

Note that Equations 10 and 11 are multiplied by the stoichiometric factors c_i and c_j before the sum is taken (which is the convention used by many researchers). The result of this formulation (which can easily be extended to third order ternary reactions) is a set of coupled differential equations that are usually solved numerically. Reference 33 gives a detailed explanation of reactions and rate laws.

There are examples in the literature of CO_2 laser discharge modeling. These models included ion reactions as well as neutral reactions. For example, Wiegand and Nighan modeled the $CO_2/N_2/He$ discharge and predicted that numerous minority species (such as those composed of carbon, oxygen, and nitrogen) are produced in significant quantities on a time scale of 100 μsec (Reference 34). These minority species are found to be directly related to the dominant ionic species. Pace and Lacome used a chemistry code to predict that when small amounts of O_2 or H_2O are present in the discharge, the negative ion population is significantly increased (Reference 13). Finally, Thoenes and Kurzius have modeled the plasma chemistry important to the formation of impurities (Reference 37). Valuable information concerning the formative reactions of impurities can be obtained from chemical modeling. This knowledge is valuable because it often leads to solutions for suppressing the impurities.

The chemical code used to model the discharge was developed by Stamm (Reference 20). The resultant differential equations were obtained by considering the reactions listed in Table 1 and were solved by the modified Euler method. However, certain assumptions and adjustments had to be made in order to obtain a model in agreement with experiment. These assumptions and adjustments are summarized below.

The electron number density in the positive column of the discharge is assumed constant, and it can be approximately calculated from the following equation:

$$n_e = \frac{I}{ev_d A} \tag{13}$$

where I is the measured discharge current, A is the cross sectional area of the discharge tube, e is the magnitude of the electronic charge, and v_d is the drift velocity of the electrons. The drift velocity of the electrons was taken from the data in Reference 38. However, a knowledge of the reduced field in the positive column was required first. It was

TABLE 1

REACTIONS AND RATE CONSTANTS USED IN THE CHEMICAL MODEL

No.	REACTION	RATE CONSTANT ($300^{o}K$)	REFERENCE
	BINARY		
1.	$e^{-}+CO_2 \rightarrow CO+O+e^{-}$	See Text	
2.	$e^{-}+CO \rightarrow C+O^{-}$	$3x10^{-14} cm^3 s^{-1}$	36
3.	$e^{-}+O_2 \rightarrow 2O+e^{-}$	$1x10^{-9} cm^3 s-1$	36
4.	$e^{-}+N_2 \rightarrow 2N+e^{-}$	See Text	
5.	$e^{-}+NO \rightarrow N+O^{-}$	$1x10^{-12} cm^3 s^{-1}$	36
6.	$N+O \rightarrow NO$	$2x10^{-17} cm^3 s^{-1}$	20
7.	$N+NO \rightarrow N_2+O$	$2.7x10^{-11} cm^3 s^{-1}$	39
8.	$N+N \rightarrow N_2$	$9x10^{-18} cm^3 s^{-1}$	20
9.	$N+O_2 \rightarrow NO+O$	$2.8x10^{-19} cm^3 s^{-1}$	39
10.	$N+NO_3 \rightarrow NO+NO_2$	$5.7x10^{-13} cm^3 s^{-1}$	39
11.	$N+O_3 \rightarrow NO+O_2$	$5.7x10^{-13} cm^3 s^{-1}$	39
12.	$O+O_3 \rightarrow 2O_2$	$8.5x10^{-15} cm^3 s^{-1}$	39
13.	$O+NO_3 \rightarrow O_2+NO_2$	$5.7x10^{-13} cm^3 s^{-1}$	39
14.	$NO+NO_3 \rightarrow 2NO_2$	$8.7x10^{-12} cm^3 s^{-1}$	39
15.	$NO+O_3 \rightarrow NO_2+O_2$	$1.6x10^{-14} cm^3 s^{-1}$	39
16.	$NO_2+O_3 \rightarrow NO_3+O_2$	$3.2x10^{-17} cm^3 s^{-1}$	39
17.	$O+NO_2 \rightarrow O_2+NO$	$9.2x10^{-12} cm^3 s^{-1}$	39
18.	$NO_2+NO_3 \rightarrow NO_2+O_2+NO$	$1.1x10^{-15} cm^3 s^{-1}$	39
19.	$NO_3+NO_3 \rightarrow 2NO_2+O_2$	$2.1x10^{-16} cm^3 s^{-1}$	39
20.	$N+NO_2 \rightarrow 2NO$	$1.4x10^{-12} cm^3 s^{-1}$	39
21.	$N+CO_2 \rightarrow NO+CO$	$1.0x10^{-19} cm^3 s^{-1}$	39
	TERNARY		
22.	$N+O+M^{*} \rightarrow NO+M$	$1.0x10^{-32} cm^6 s^{-1}$	39
23.	$N+N+M \rightarrow N_2+M$	$4.4x10^{-33} cm^6 s^{-1}$	39
24.	$O+NO_2+M \rightarrow NO_3+M$	$9.6X10^{-32} cm^6 s^{-1}$	39
25.	$N+NO+M \rightarrow N_2O+M$	$1.0x10^{-35} cm^6 s^{-1}$	20
26.	$O+O+M \rightarrow O_2+M$	$7.2x10^{-33} cm^6 s^{-1}$	39
27.	$O+NO+M \rightarrow NO_2+M$	$9.4x10^{-32} cm^6 s^{-1}$	39
28.	$O+O_2+M \rightarrow O_3+M$	$5.4x10^{-34} cm^6 s^{-1}$	39
29.	$O+CO+M \rightarrow CO_2+M$	$2.4x10^{-36} cm^6 s^{-1}$	39

*ALL SPECIES

calculated approximately by the following procedure. The electric field was determined by subtracting the total tube voltage from the cathode fall of potential and dividing this voltage difference by the length of the positive column. The electric field was then divided by the gas number density in order to arrive at a value of the reduced field.

From the reactions considered, the rate for CO_2 dissociation by electron impact was the most dominant term in the total rate equation for CO_2. However, the published value of the rate constant for CO_2 dissociation (e.g. Reference 36) did not result in CO_2 dissociation in agreement with experiment. The code prediction of CO_2 dissociation was far greater than that actually observed. A rate constant providing agreement with experiment was obtained in the following way. It was determined that the CO_2 rate equation could be approximated by

$$\frac{d[CO_2]}{dt} = -k[CO_2]\, n_e \tag{14}$$

Integrating Equation 14 and applying the initial condition that at t=0, $[CO_2] = [CO_2]_o$, the following result is obtained:

$$[CO_2] = [CO_2]_o\, e^{-knet} \tag{15}$$

Solving for the rate constant and using a time of 1 sec (which is consistent with the gas residence time).

$$k = \frac{1}{n_e}\, \ell n\, \frac{[CO_2]_o}{[CO_2]} \tag{16}$$

$[CO_2]_o$ and $[CO_2]$ can be obtained from experiment, and n_e can be calculated by the procedure mentioned previously. The rate constant, calculated by using Equation 16, was used in the code so that the theoretical curve for CO_2 concentration versus discharge current is made to fit the

experimental one. The concentration of all other species were compared with the experimental values with the above adjustment made to the CO_2 dissociation rate constant.

SECTION IV

EXPERIMENTAL RESULTS AND COMPARISON WITH THEORY

The voltage-current characteristics of the mixtures used in the synthesis experiment are shown in Figure 4. The Ar in each mixture was used for calibration purposes and its concentration was approximately 10% (see Appendix C). Using the CO_2/Ar curve as a reference, it can be seen that N_2/Ar and CO_2/N_2/Ar discharges operated at higher sustaining voltages while CO_2/He/Ar and CO_2/N_2/He/Ar discharges operated at lower ones. This difference is explained by the following material.

The sustaining voltage of a glow discharge depends inversely on the ionization coefficient which is defined as the number of ion pairs formed by an electron per volt in the direction of the field (Reference 40). (The sustaining voltage also depends on the secondary emission coefficient which appears in a relatively slow varying term.) The ionization coefficient depends on the nature of the gas and the reduced field of the discharge (References 23 & 40). The reduced field of the N_2/Ar discharge is calculated to be 5.5 Td using the method described in the previous section. Consequently, there is approximately an 85% probability that a N_2 molecule is vibrationally excited; and the probability of ionizing a N_2 molecule is vanishingly small (see Figure 9). Although the result in Figure 9 is for the fractional power transfer in a N_2 discharge, it can be translated into the probability of occurrence of the processes shown as a function of the reduced field. Since N_2 constitutes 90% of the mixture and the ionization of N_2 contributes little to the ionization coefficient, it can be seen why the sustaining voltage is higher. Also, according to Figure 9, the formation of ion pairs by the metastable reactions (Reference 41)

$$N_2^* + e^- \rightarrow N_2^+ + 2e^- \qquad (17)$$

and

$$N_2^* + e^- \rightarrow N^+ + N + 2e^- \qquad (18)$$

is not highly probable; and further evidence showing that Equation 18

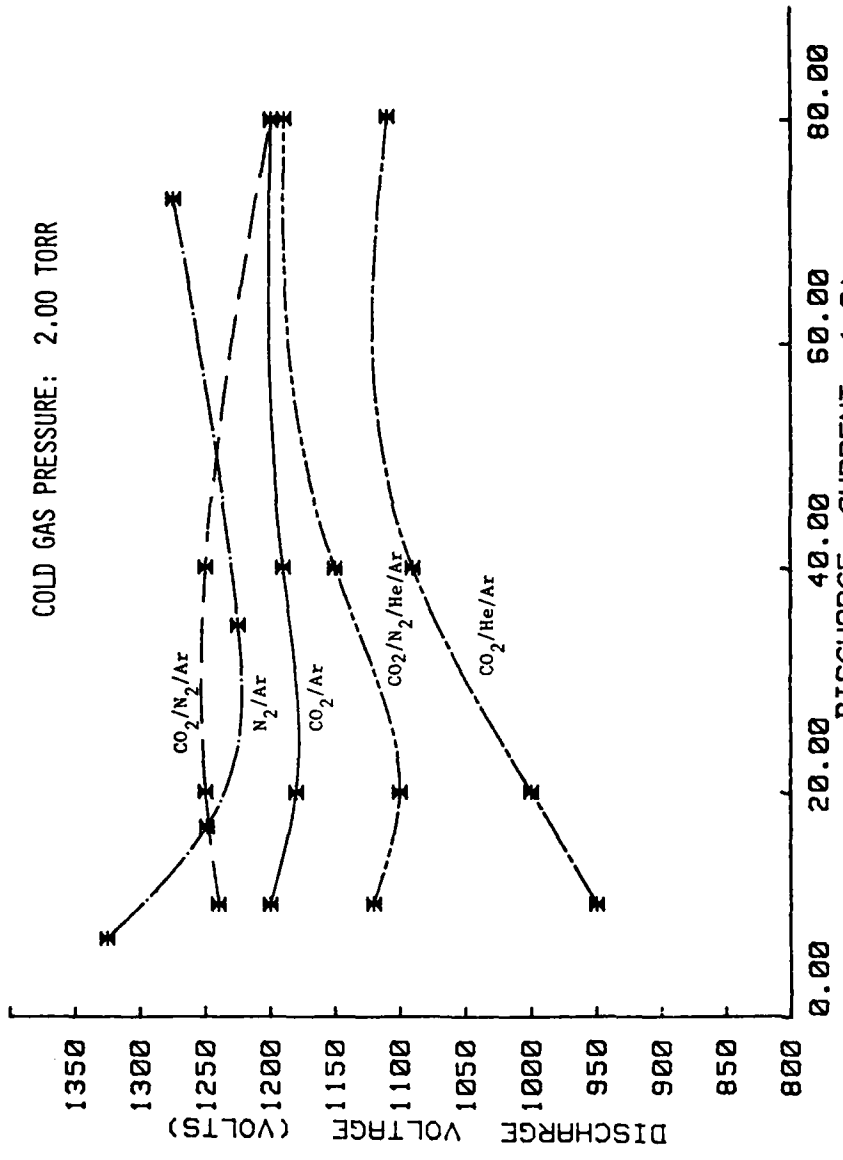

Figure 4. Voltage-Current Characteristics

has a low probability of occurring is that there is little or no dissociation in a N_2/Ar discharge (Reference 22).

It is obvious that the high sustaining voltage of the $CO_2/N_2/Ar$ discharge is the result of a low ionization coefficient. Hence, there is very little ion pair formation occurring. Whether the discharge is mostly vibrationally or electronically excited is unknown because of the inavailability of data such as that in Figure 9.

When He is added to CO_2/Ar and $CO_2/N_2/Ar$, there is a resultant increase in the ionization coefficient. This increase is due to the following Penning reactions (References 40 and 42):

$$He^* + Ar \rightarrow Ar^+ + e^- + He \qquad (19)$$

$$He\ (2^3s) + N_2 \rightarrow N_2^+ + e^- + He \qquad (20)$$

As a result, the sustaining voltage is lowered considerably.

Figure 5 shows the discharge pressure as a function of current. The pressure increased with current in all of the mixtures except that of N_2/Ar. In the case of N_2/Ar, the pressure dropped by 0.01 Torr and remained constant over the entire range of current values (10-70 mA). This pressure drop has also been observed by Karube and Yamaka in the case of a sealed-off N_2 discharge (Reference 6). If the gas mixture is inert, gas heating and electrophoresis are the principle causes of the pressure change; and if the mixture is chemically active under discharge conditions, dissociation must be included as one of the causes.

Figures 6, 7, and 8 summarizes the neutral chemistry of a CO_2/Ar discharge. The average rate constant (i.e. calculated from Equation 16) for CO_2 dissociation is 5.4×10^{-11} cm^3 s^{-1}. Using this rate constant in the chemical code, the experimental and theoretical CO_2 concentrations in Figure 6 agree favorably as expected. The experimental fractional

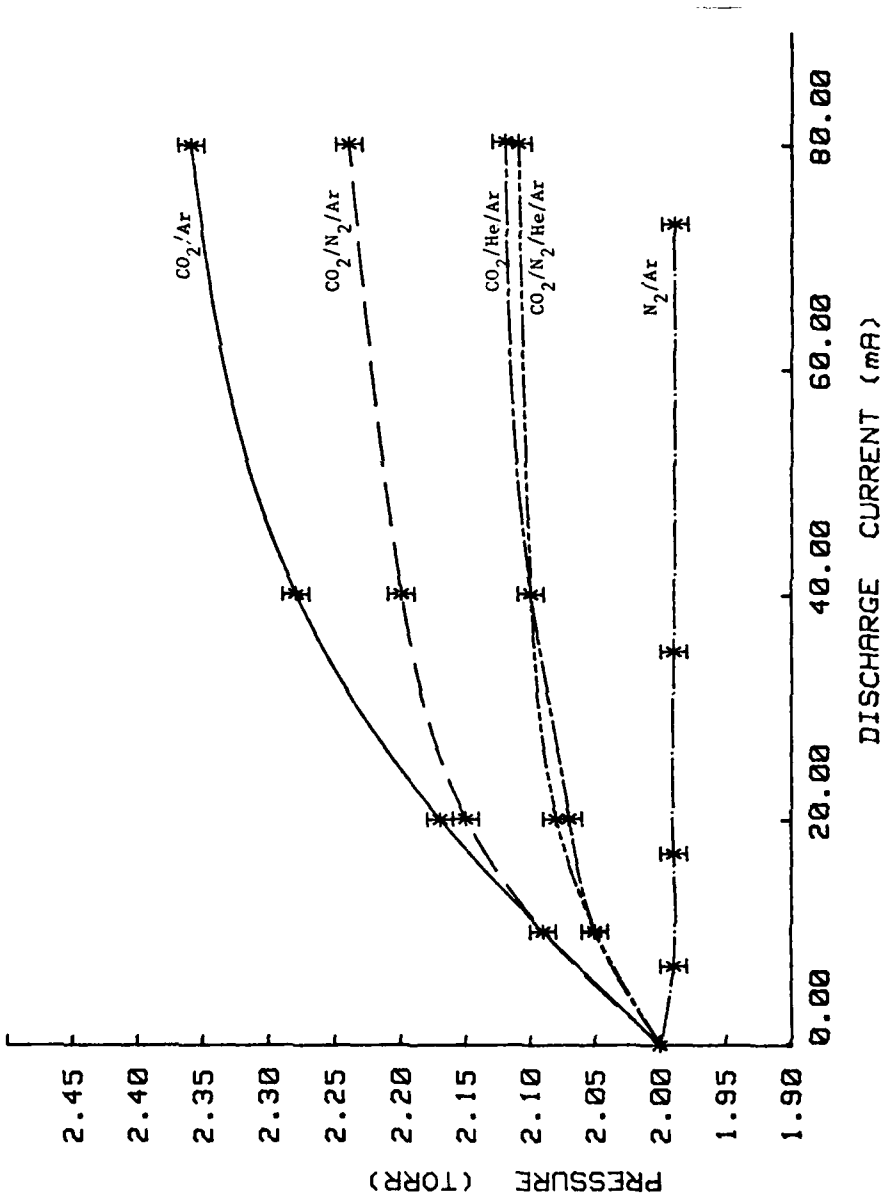

Figure 5. Pressure Variations

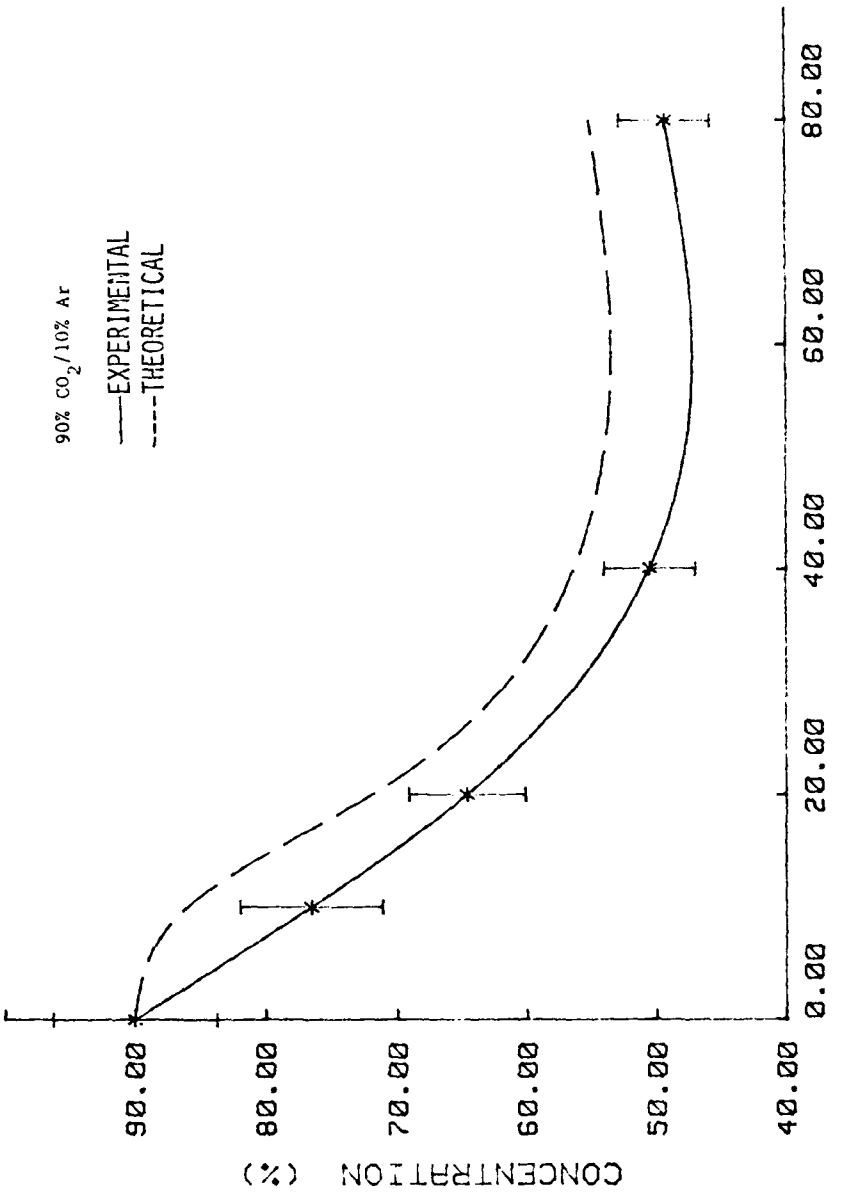

Figure 6. CO_2 Concentration in a CO_2/Ar Discharge

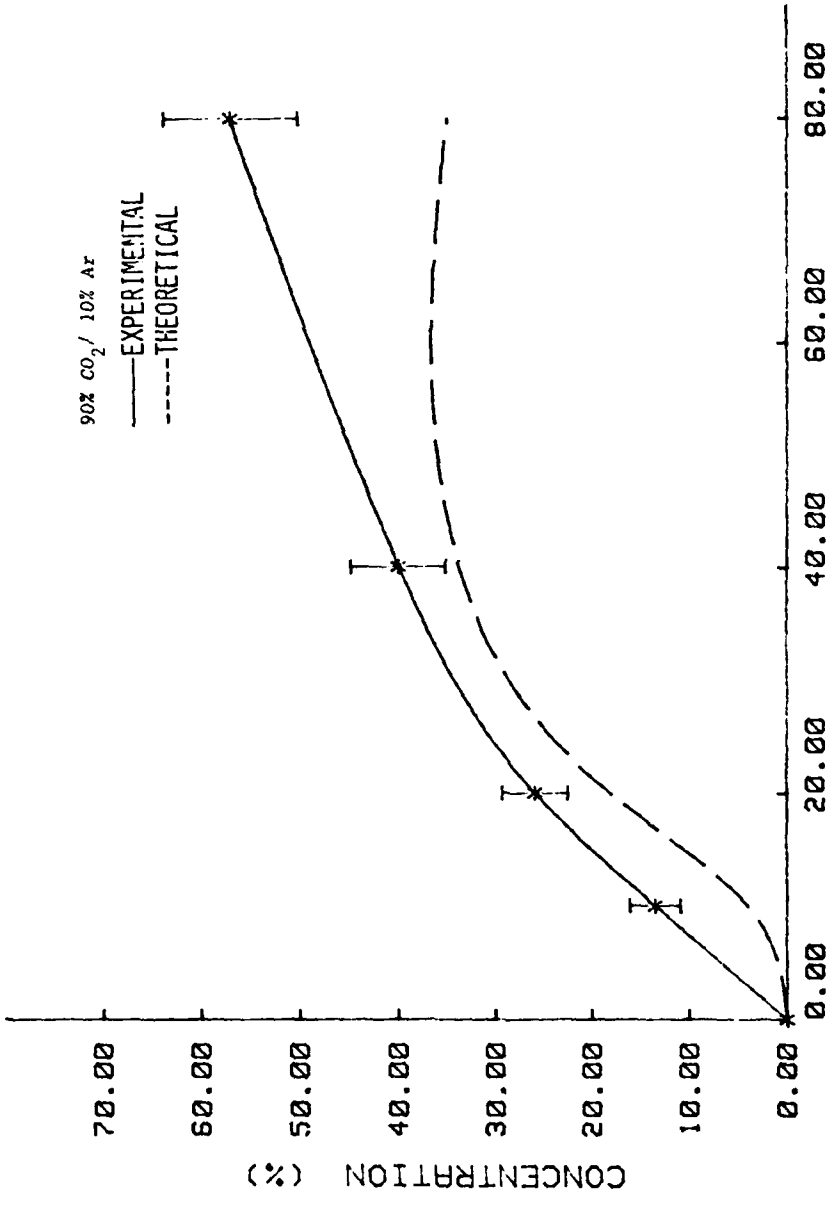

Figure 7. CO Concentration in a CO_2/Ar Discharge

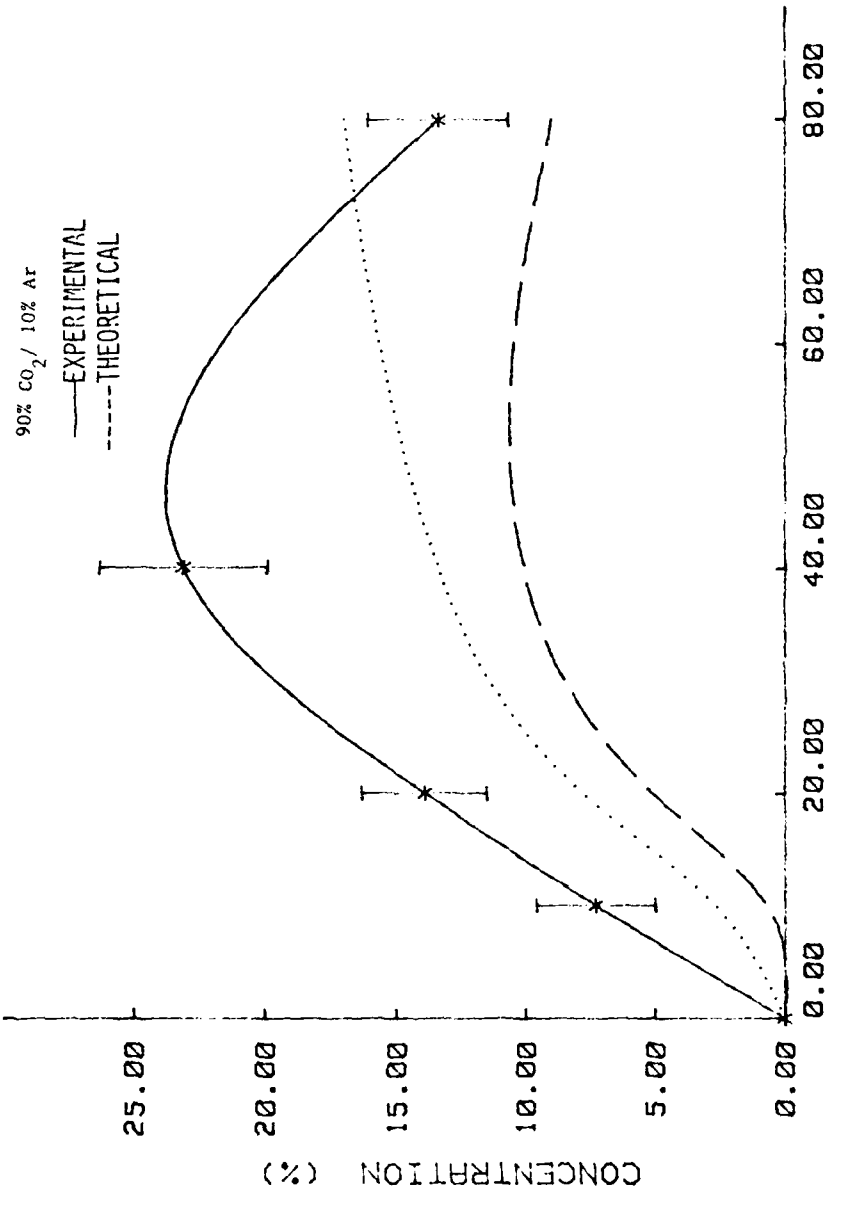

Figure 8. O_2 Concentration in a CO_2/Ar Discharge

The dotted curve is the theoretical prediction of the atomic oxygen concentration.

dissociation of CO_2 was 44%. Buser and Sullivan has shown that dissociation up to 80% is common (Reference 5). Dissociation is preceeded by the production of an electronic excited state of CO_2 by electron impact (Reference 7):

$$CO_2 + e^- \rightarrow CO_2\ (^3\pi) + e^- \qquad (21)$$

with subsequent dissociation occurring through the following reaction:

$$CO_2\ (^3\pi) + e^- \rightarrow CO + O + e^- \qquad (22)$$

Dissociation can also occur through dissociative attachment (Reference 36):

$$CO_2 + e^- \rightarrow CO + O^- \qquad (23)$$

The overall rate constant for the mechanism illustrated in Equation 21 and Equation 22 is 1×10^{-9} cm^3 s^{-1} (300°K), while that of Equation 23 is 5×10^{-13} cm^3 s^{-1} (300°K) (Reference 36). The calculated rate constant for CO_2 dissociation lies between those of dissociation by electron impact and dissociative attachment. This calculated rate constant is larger than that of dissociative attachment by a factor of 10^3.

With a large dissociation of CO_2, there should be a large formation of CO. This was indeed the case as shown in Figure 7. There should also be atomic and molecular oxygen, and the concentration of O should be larger than that of O_2 since the rate constant for CO_2 dissociation is much larger than that of the three body recombination of O (see Table 1). This behavior is exactly what is predicted by the code (Figure 8). However, O_2 was the only form of oxygen detected experimentally in all of the mixtures.

The absorption of atomic oxygen on the walls of the discharge tube is a possible mechanism by which it is lost. Atomic oxygen can also recombine on the walls of the discharge tube forming O_2; hence, the "effective" rate for O recombination is larger than that shown in Table 1. This adjustment was not included in the code.

No detectable dissociation of N_2 was observed in a N_2/Ar discharge. This observation is supported by the fact that there was no N signal and no change in the N_2 signal. The N_2/Ar discharge operated at a reduced field of 5.5 Td; hence, the probability of vibrationally exciting N_2 is much greater than that of dissociation (see Figure 9).

The neutral chemistry of a CO_2/N_2/Ar discharge is illustrated in Figures 10, 11, and 12. The CO_2 and N_2 percentages were 40% and 50%, respectively. The fractional dissociation of CO_2 was approximately 63%, and it was greater than that in the case of a CO_2/Ar discharge.

As in the case of CO_2/Ar, there was no indication of CO dissociation at high discharge currents because there was no carbon (C) signal. The experimental CO percentage in Figure 11 is slightly higher than that shown. The reason is that CO and N_2 have approximately the same mass number, and a constant N_2 signal (which was determined from the mixture with the discharge off) was subtracted from the total signal at mass number 28 in determining the CO signal. Resolution constraints did not permit an accurate determination of the CO and N_2 signals. However, there was N_2 dissociation ($\sim$1%), and it was deduced from a rise in the atomic nitrogen (N) signal and from the formation of nitric oxide (NO). Therefore, subtraction of a constant N_2 signal from the CO signal is not fully justified, but it represents a fair approximation.

The only nitrogen oxide detected was NO, and the concentration of NO stayed at a constant 0.3% of the total ion current from the spectrometer in the range from 20 to 80 mA. Nitrogen dioxide (NO_2) was not

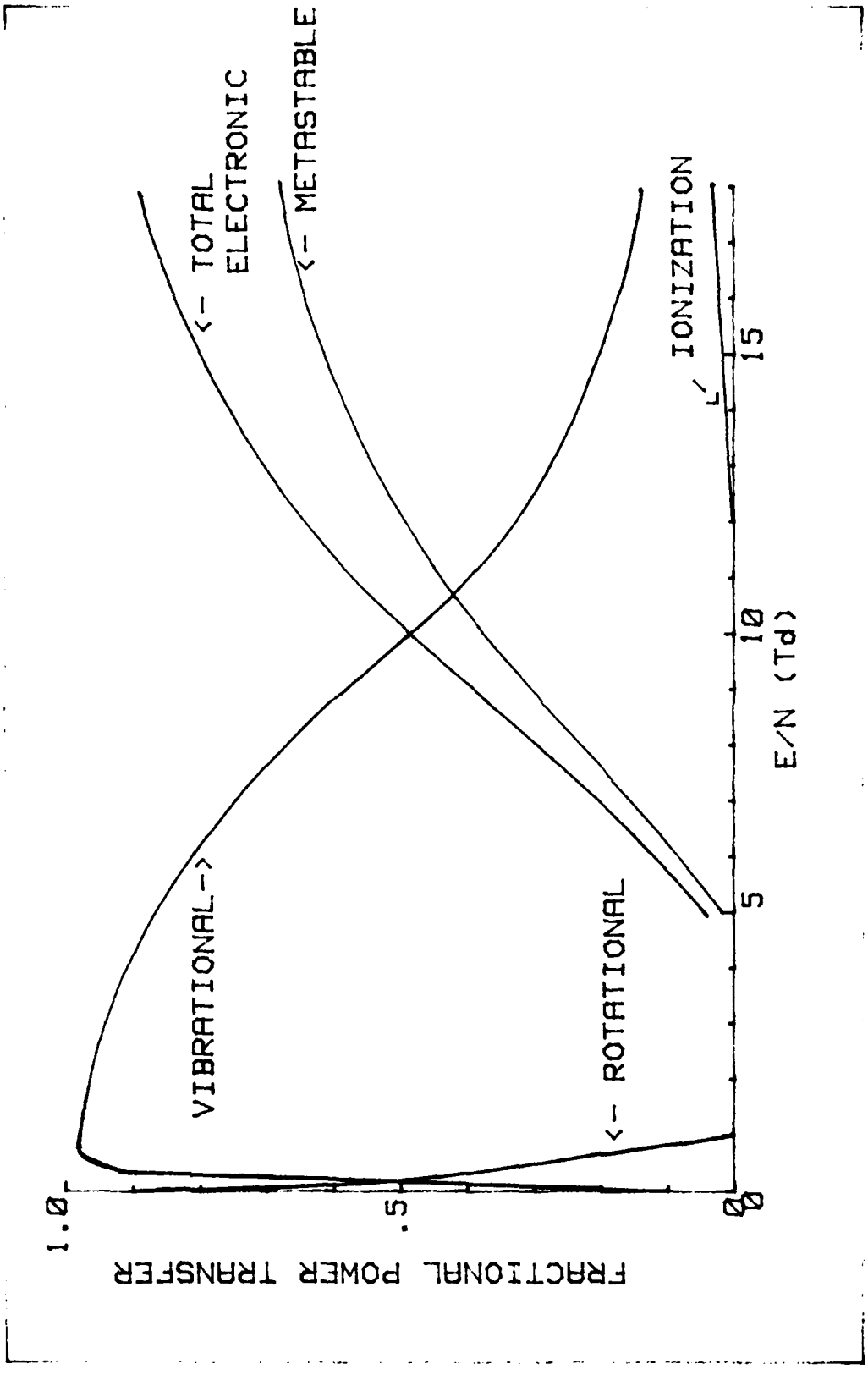

Figure 9. Fractional Power Transfer in a N_2 Discharge (Refe e 46)

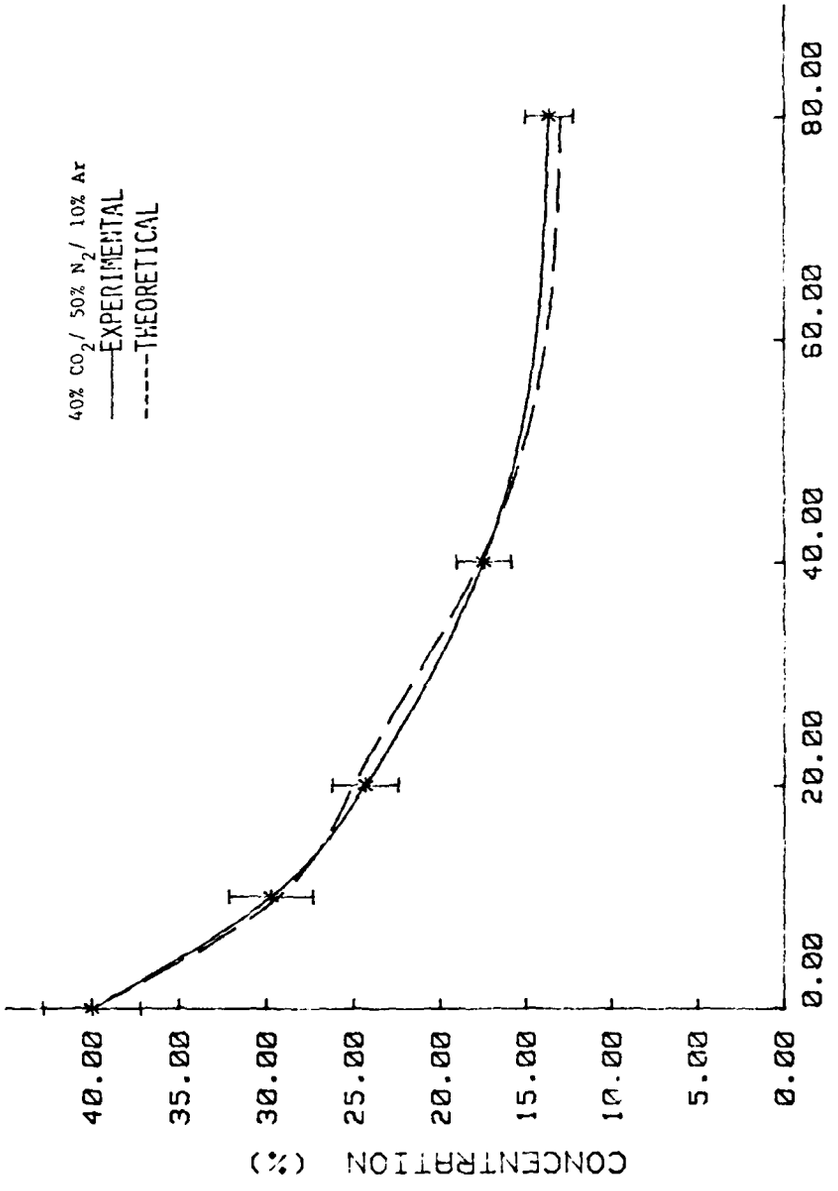

Figure 10. CO_2 Concentration in a $CO_2/N_2/Ar$ Discharge

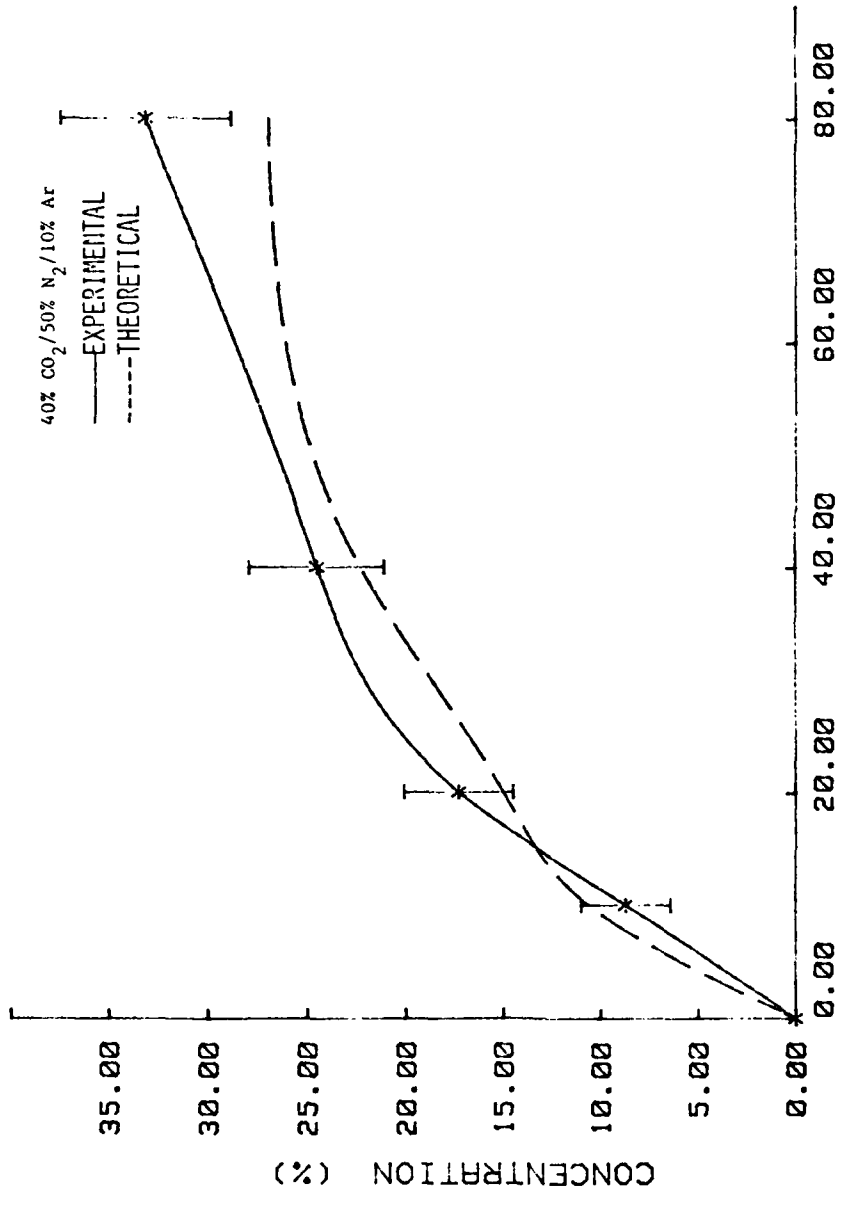

Figure 11. CO Concentration in a $CO_2/N_2/Ar$ Discharge

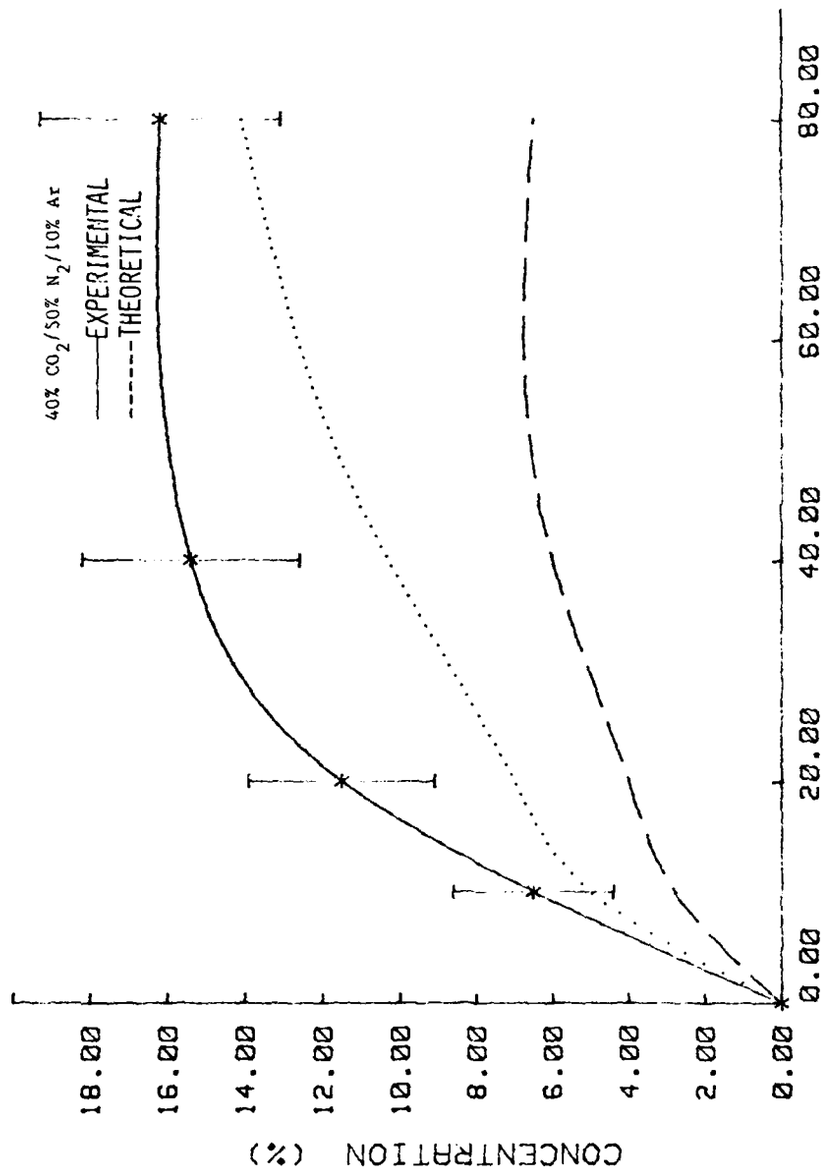

Figure 12. O_2 Concentration in a $CO_2/N_2/Ar$ Discharge

The dotted curve is the theoretical O concentration.

formed in detectable quantities, and nitrous oxide (N_2O) could not be detected because the resolution of the spectrometer is not sufficient in resolving the N_2O and CO_2 signals. The former conclusion is based on the following fact. A signal appeared at mass number 46 with no discharge, and this signal was attributed to the carbon dioxide isotopes $O^{17}\ C^{12}\ O^{17}$ and $O^{16}\ C^{12}\ O^{18}$. If NO_2 was formed, then its signal would have increased the total signal at mass number 46. However, this was not the case.

In the case of the $CO_2/N_2/Ar$ discharge, there is fair agreement between the experimental results and the results of the code. An average calculated rate constant of $1.7X10^{-10}$ cm^3 s^{-1} for CO_2 dissociation was used in the model. The code required a rate constant for the dissociation of N_2 by electron impact (reaction number 4 in Table 1). Since N_2 is very similar in mass and vibrational energy spacing as O_2 (Reference 43), the rate constant was assumed to be the same as that given for reaction number 3. The code prediction of the NO concentration was less than 5 ppm even at high discharge currents ($\sim$80 mA). The predicted N_2O and NO_2 concentrations were less than the NO concentration by factors of 10^2 and 10^3, respectively. Since there was no NO available for calibration, adequate comparison between the experimental and theoretical NO concentrations could not be made.

Figures 13 through 18 show the neutral chemistry of a $CO_2/He/Ar$ and $CO_2/N_2/He/Ar$ discharge. The fractional dissociation of CO_2 was 74% in $CO_2/He/Ar$ and up to 76% in $CO_2/N_2/He/Ar$. The corresponding calculated rate constants for CO_2 dissociation were 2.2×10^{-10} cm^3 s^{-1} and 2.3×10^{-10} cm^3 s^{-1}, respectively.

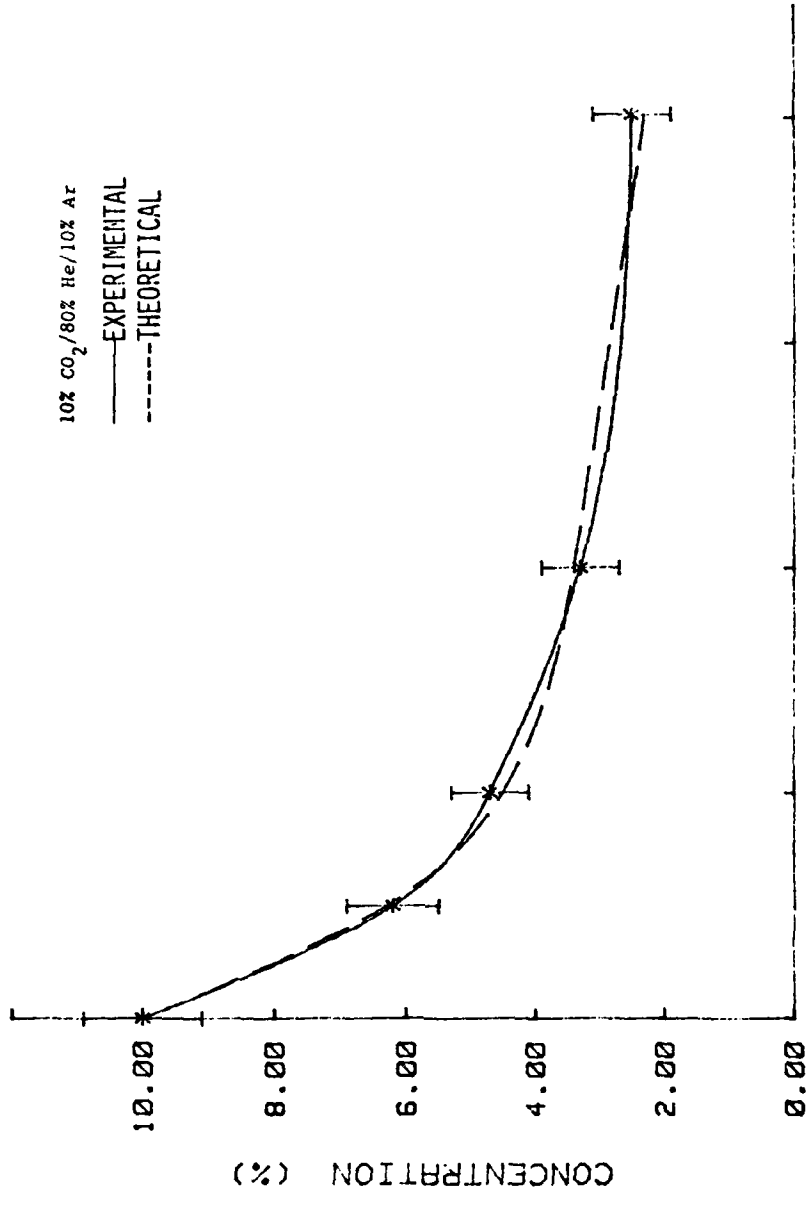

Figure 13. CO_2 Concentration in a CO_2/He/Ar Discharge

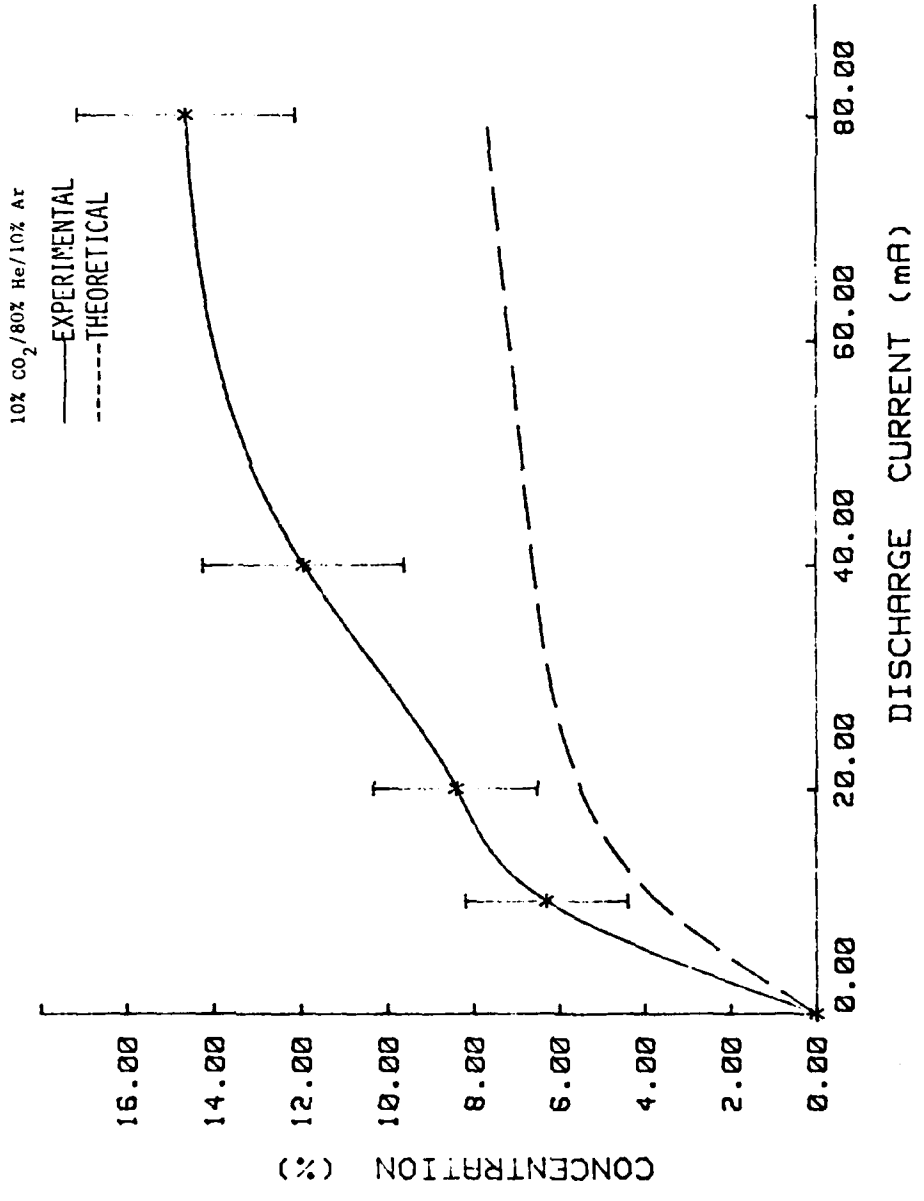

Figure 14. CO Concentration in a CO_2/He/Ar Discharge

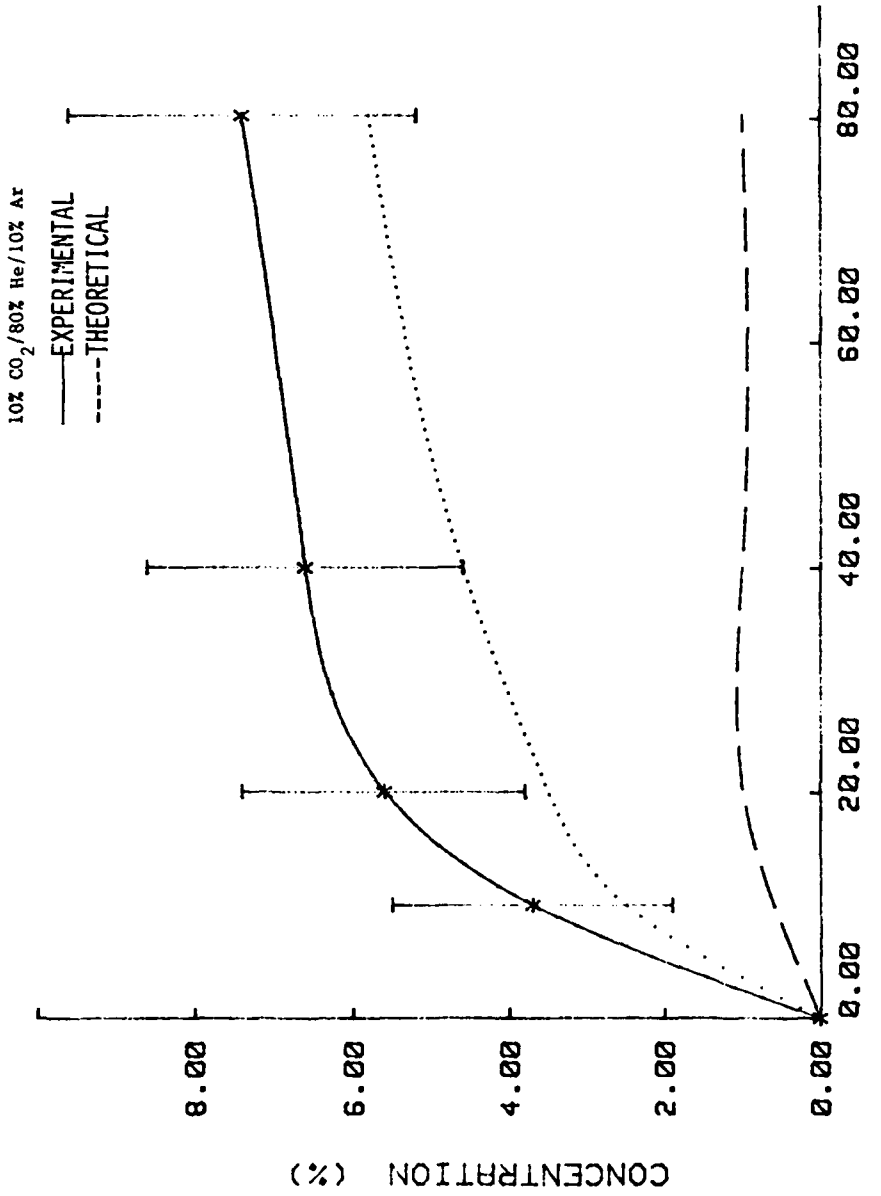

Figure 15. O_2 Concentration in a CO_2/He/Ar Discharge

The theoretical O concentration is shown as the dotted curve.

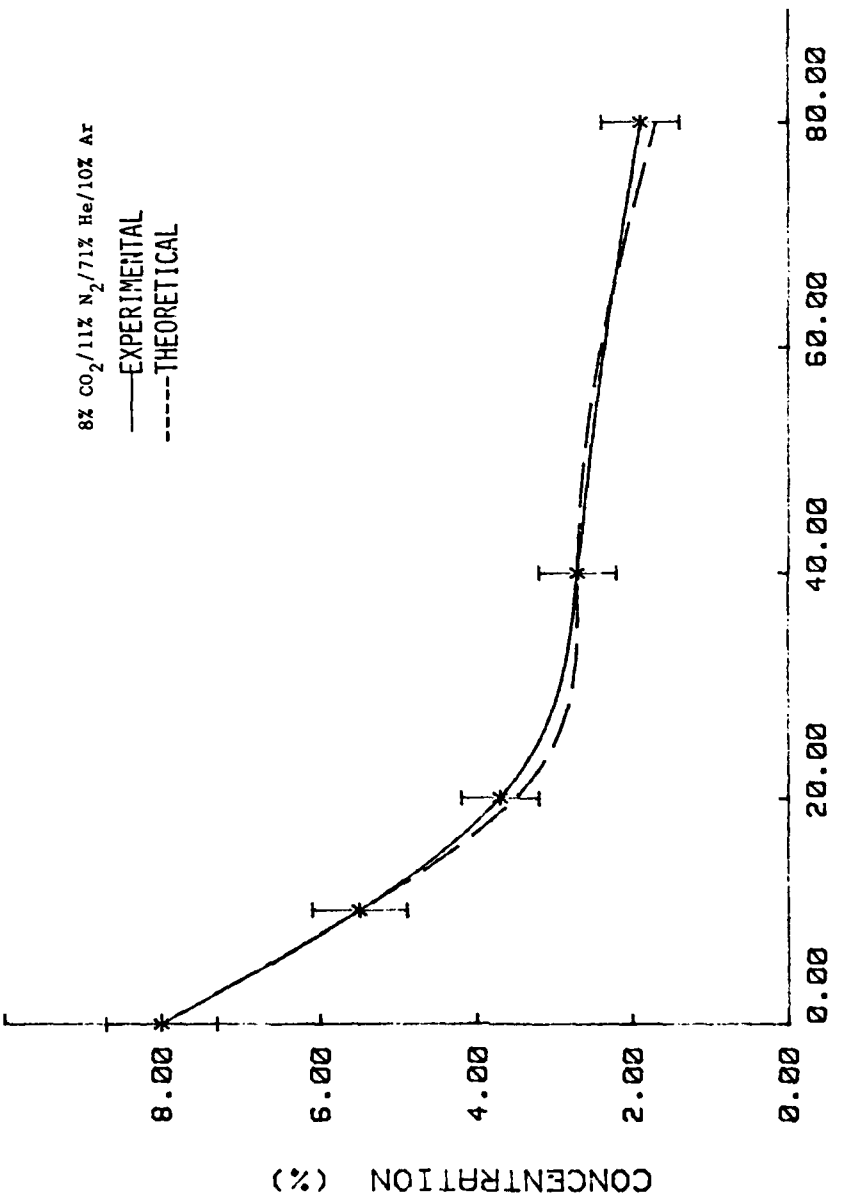

Figure 16. CO_2 Concentration in a CO_2/N_2/He/Ar Discharge

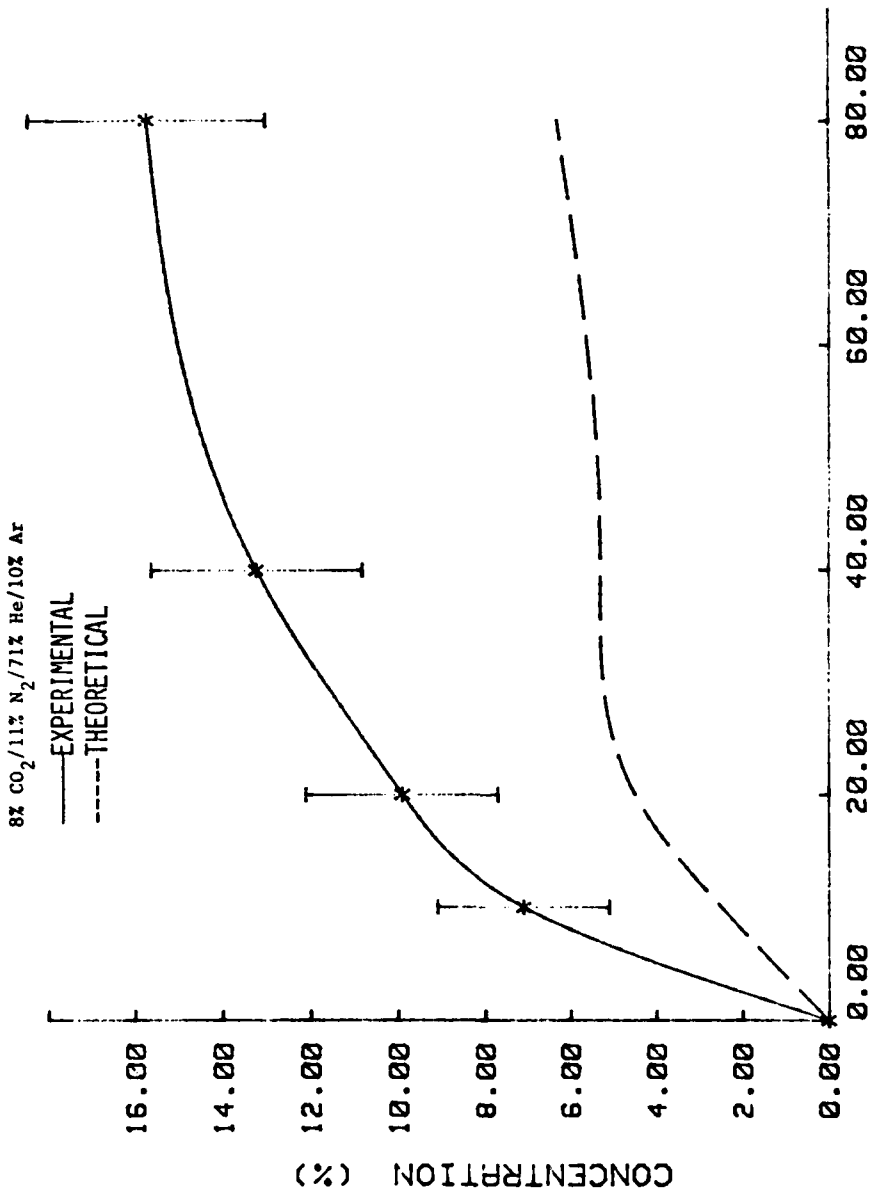

Figure 17. CO Concentration in a $CO_2/N_2/He/Ar$ Discharge

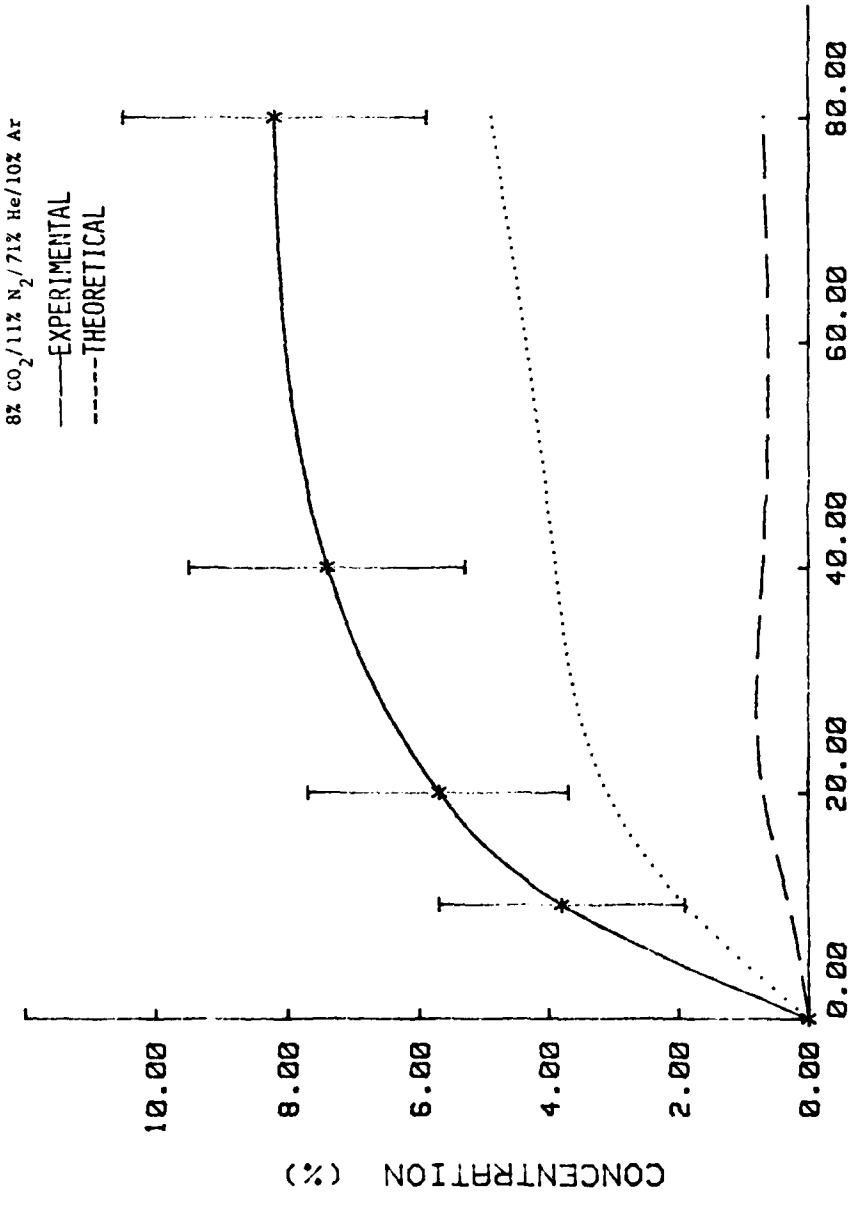

Figure 18. O_2 Concentration in a $CO_2/N_2/He/Ar$ Discharge

The theoretical atomic oxygen concentration is shown as the dotted curve,

In $CO_2/N_2/He/Ar$, small amounts of carbon (C) were detected, and the percentage of C in the spectrometer ion current fluctuated between 0.09% and 0.26%. The C may have come from the dissociation of CO; however, this is not apparent from Figure 17. The CO concentration, however, was strangely larger than the original CO_2 concentration at discharge currents greater than 20 mA. This is attributed to an error in extrapolating the spectrometer factor (see Appendix C).

N_2 dissociation occurred also in the $CO_2/N_2/He/Ar$ discharge. Consequently, NO was formed, and its concentration stayed at a constant 0.5% of the total ion current over the whole range of the discharge current (10-80 mA). There was no trace of NO_2, and the presence of N_2O could not be detected because of its similarity in mass with that of CO_2. The maximum NO concentration that the code predicted was approximately 2 ppm with N_2O and NO_2 at concentrations of 5 ppb and 1 ppb, respectively.

The ion chemistry and the effects of H_2 in a CO_2 laser discharge has also been studied. These results have been published elsewhere (References 3, 14, 15 and 19), and only a brief summary will be given here.

sitive ions were sampled from the afterglow behind a hollow cylindrical cathode in a 12.78% CO_2/87.22% He and 12.7% CO_2/15.5% N_2/ 71.8% He discharge. In both cases, the total gas pressure was 2 Torr and the discharge current was 40 mA. The major positive ions in the $CO_2/N_2/He$ mixture were CO_2^+, O_2^+, CO^+, N_2^+, C^+, N^+, O^+, and NO^+; while CO_2^+, O_2^+, O^+, and C^+ were observed in CO_2/He (Reference 3). Chemical equilibrium of all of the positive ion species was reached in approximately 10 seconds after the discharge was turned on.

Negative ions were sampled from the afterglow behind a hollow cylindrical anode in a 12.7% CO_2/ 15.5% N_2/ 71.8% He discharge. Changes in the relative composition of the negative ions were observed in a current range from 0.2 to 60 mA. The gas residence time was 62 milliseconds, and the total gas pressure was 1 Torr. The major negative ions were NO_2^-, NO_3^-, O_2^-, O^-, and CO_3^- (Reference 15). The following ions were also present: OH^-, HCO_3^-, CHO^-, and trace amounts of CN^-. The dominant negative ion was NO_2^- while CO_3^- was observed to be dominant only at low values of the discharge current. Chemistry code calculations indicate CO_3^- as being dominant regardless of the current range (Reference 36). However, if the nitrogen oxides (NO, N_2O, and NO_2) are added in the code calculations, the dominant ion would be NO_2^- in agreement with what is observed experimentally (Reference 35). Negative ions can also be suppressed by the addition of CO to the discharge (Reference 14). The CO detaches O^- from negative ions such as CO_3^-, NO_2^-, and NO_3^-.

With the addition of 2% H_2 to a 75% N_2/15% CO_2/ 10% Ar discharge, the contaminants O_2 and NO were reduced. CO_2 dissociation was reduced by as much as 20% at high values of the discharge current (80 mA) (Reference 19). The tradeoff is that as H_2 is added, the production of the contaminant species H_2O increases.

SECTION V

CONCLUSIONS

CO_2 dissociation is the fundamental problem in closed-cycle CO_2 lasers because the dissociation products lead to the formation of contaminants. The dissociation of N_2 also aids in the formation of contaminants, but N_2 dissociation only occurs in the presence of CO_2 which acts as a catalyst. The dissociation energy of ground state CO_2 into ground state products has been previously reported as 5.5 ev (Reference 5). The dissociation energy of N_2 has been reported to be approximately 7-10 ev (Reference 44). Hence, it is unlikely that N_2 dissociation occurs through the interaction of N_2 with vibrationally excited CO_2 since the dissociation energy of N_2 is higher than that of CO_2. The dissociation products of CO_2, which are CO and O_2, are very similar in mass and vibrational energy spacing to N_2 (Reference 43). The dissociation energies of CO and O_2 are approximately 9-11 ev and 5.08 ev, respectively (Reference 44). O_2 would dissociate before it acquired enough vibrational energy to dissociate N_2 since the dissociation energy of O_2 is about half that of N_2. However, it is energetically possible for vibrationally excited CO to dissociate N_2.

CO_2 dissociation occurs by electron impact and/or dissociative attachment. The calculated rate constant from Equation 16 and the experimental data, assuming an exponential decay of CO_2, lies between the published values of the rate constant for electron impact dissociation and dissociative attachment. In the four mixtures used in the synthesis experiment, the calculated rate constant differed from the published value of 1×10^{-9} cm^3 s^{-1} for electron impact dissociation by a factor of approximately 20. However, it was larger than the rate

constant for dissociative attachment by a factor of 10^3. Therefore, it can be concluded that the dissociation of CO_2 occurs primarily by electron impact. Although the low concentration of O^- would seem to confirm this conclusion, it cannot be used as exclusive proof since O^- clusters rapidly to form negative ions (References 14 and 15).

The code predicts that O is larger than O_2 in all mixtures, but O_2 was the only form of oxygen that was observed experimentally. The reason that the code predicts such a high concentration of O is because the recombination rate of O to form O_2 did not include wall recombination. The recombination rate includes only third body reaction with the other molecules of the discharge (see reaction number 26 in Table I). Another reason why the code predicts high O concentrations is due to the fact that the code does not include ion chemistry to take into account the formation of O^-.

In pure CO_2 or CO_2/He discharges at low pressure, the following positive ion producing reaction is expected:

$$e^- + CO_2 \rightarrow CO_2^+ + 2e^- \qquad (24)$$

The positive ions O^+ and O_2^+ are subsequently formed by fast charge transfer reactions with CO_2^+ in addition to electron impact ionization of O and O_2:

$$CO_2^+ + O \rightarrow O^+ + CO_2 \qquad (25)$$

$$CO_2^+ + O_2 \rightarrow O_2^+ + CO_2 \qquad (26)$$

Reactions 24, 25, and 26 suggest that CO_2^+, O^+, and O_2^+ would be among the dominant ions formed in a CO_2/He discharge. This conclusion is indeed the case experimentally (Reference 3). In CO_2/N_2 and CO_2/N_2/He discharges,

the dominant impurity positive ion is NO^+ which is not surprising since NO is the dominant impurity formed (References 3 and 22).

Unlike positive ions, negative ions can affect the stability of the discharge if their concentration becomes large (Reference 13). CO can be added to the discharge as a detacher which limits the population of the negative ions (Reference 14). The trade-off is that the additional CO competes with the CO_2 for vibrational excitation, and N_2 dissociation may increase by the interaction of excited CO with N_2. As a consequence of N_2 dissociation, various nitrogen oxides are produced which are also quenchers of excited CO_2. Again, since NO is the dominant neutral impurity in a $CO_2/N_2/He$ discharge and O^- clusters very rapidly to NO forming NO_2^-, it can be seen why the latter is the dominant negative ion.

The added H_2 in a CO_2 laser mixture intercepts the oxygen produced by CO_2 dissociation, thereby, limiting the amount of impurity species formed. The most notable of these impurity species is NO. H_2 also decreases the amount of CO_2 dissociation which is very desirable for long-term sealed operation of the CO_2 laser.

It is emphasized that optimum conditions cannot be determined from studying the plasma chemistry alone, but a study of other laser parameters such as output power need to be considered. For this reason, there is a need for on-line capabilities to actual laser systems which include sampling from high pressure discharge lasers.

APPENDIX A

RESIDENCE TIME AND PARTIAL PRESSURE CALCULATION

Consider a tube of circular cross section. Assuming Poiseuille flow through this tube, the radial velocity profile is parabolic. As a result, the gas near the walls have a slower velocity and thus stay in the discharge longer. It is the gas near the walls that the spectrometer samples because the sampling orifice is located at the wall. In the following discussion, it is assumed that all the molecules travel through the tube at the same rate.

The volume of gas that passes an imaginary plane perpendicular to the flow in time Δt is given by

$$\Delta V = v\, \Delta t\, A \tag{A.1}$$

where v is the velocity of the flow, and A is the cross sectional area of the tube which is assumed constant. Solving for the flow velocity in Equation A.1, the following result is obtained:

$$v = \frac{\Delta V}{\Delta t A} \tag{A.2}$$

$\frac{\Delta V}{\Delta t}$ is the volume flow rate past an imaginary plane within the tube. This flow rate is usually given in standard cubic centimeters per minute (SCCM). A standard cubic centimeter is the volume occupied by a given gas at standard temperature and pressure (STP). Standard temperature and pressure are defined as 20°C and 760 mm of Hg (torr), respectively. Assuming an ideal gas, the number density of molecules in one standard cubic centimeter is given by

$$n_o = \frac{p_o}{kT_o} = 2.505 \times 10^{19}\ \text{cm}^{-3} \tag{A.3}$$

where p_o and T_o are the standard values of pressure and temperature, respectively; and k is Boltzmann's constant.

If the temperature is constant, then the volume occupied at any arbitrary pressure p is given by

$$\Delta V = \frac{p'}{p} \Delta V' \tag{A.4}$$

where $\Delta V'$ is the volume occupied at any other arbitrary pressure p'. If $p' = p_o$, then $\Delta V'$ is the volume occupied at standard pressure. Substituting ΔV from Equation A.4 into Equation A.2 with $p' = p_o$, the flow velocity becomes

$$v = \frac{\Delta V' \; p_o}{\Delta t A \; p} = \frac{H \; P_o}{A \; p} \tag{A.5}$$

where $H = \frac{\Delta V'}{\Delta t}$. H is the standard flow rate given in SCCM.

The residence time is defined as the length of time that a portion of the gas is in the discharge before it is sampled by the spectrometer. The residence time is given by

$$\tau = \frac{\ell}{v} \tag{A.6}$$

where ℓ is the length that the gas travels in the discharge before it reaches the sampling orifice. Substituting the flow velocity from Equation A.5 into Equation A.6, the residence time becomes

$$\tau = \frac{A \ell p}{H p_o} \tag{A.7}$$

When the flow of gas through the discharge tube reaches steady state, the pressure remains constant and the flow in is equal to the flow out. Under this condition of steady state, the total number of molecules in the experimental region of interest (i.e., from the point where it is sampled by the spectrometer) is given by

$$N = n_o H \tau \tag{A.8}$$

where τ is the residence time of the gas, H is the total flow rate in

SCCM, and n_o is the number density of molecules in a standard cubic centimeter. If the flow contains a mixture of gases, then the total flow rate is just the sum of the individual flow rates of all the gases that constitute the mixture:

$$H = \sum_s H_s \tag{A.9}$$

The total number density is

$$n = \frac{N}{A\ell} = \frac{n_o H \tau}{A \ell} \tag{A.10}$$

Similarly, the number density of species s is given by

$$n_s = \frac{n_o H_s \tau}{A \ell} \tag{A.11}$$

The fractional amount of species s is obtained by dividing A.11 by A.10:

$$\frac{n_s}{n} = \frac{H_s}{H} \tag{A.12}$$

Finally, assuming an ideal gas, the partial pressure of species and the total pressure is proportional to the number density of species s and the total number density, respectively:

$$\frac{p_s}{p} = \frac{H_s}{H} \tag{A.13}$$

APPENDIX B

THE ELECTRIC MASS FILTER

Paul and Steinwedel (Reference 24) in Germany, and R.F. Prost in the United States proposed that ions of different charge to mass ratios can be separated by a high-frequency quadrupole electric field. This method was tested (Reference 25), and a more accurate investigation was done (Reference 26). The following discussion represents a summary of the important aspects of a mass filter.

The mass filter is constructed ideally of four parallel electrodes of hyperbolic cross section in a square array (refer to the top of Figure 19). If a potential + Φ_o is applied to one set of opposite electrodes and - Φ_o to the other set, a hyperbolic electric potential between the electrodes is the result. The potential is symmetric, two dimensional (i.e. independent of z), and the potential on the z axis is zero. The potential is described in general by

$$\Phi = \Phi_o (\alpha x^2 + \beta y^2) \qquad (B.1)$$

where α and β are constants, and Φ_o is the magnitude of the potential given to the electrodes. $\Phi_o = U + V \cos \omega t$ where U is a D.C. voltage, V is the peak amplitude of a radio - frequency (rf) voltage, and $\omega = 2\Pi f$ where f is the frequency of the rf voltage. In practice, the potential is approximated by replacing the hyperbolic electrodes with cylindrical electrodes (shown at the bottom of Figure 4). This approximation is good in the region near the axis of the mass filter.

In the space between the electrodes, $\nabla^2\Phi = 0$ so that $\nabla^2\Phi = 2\Phi_o (\alpha + \beta) = 0$. Since $\Phi_o \neq 0$, then $\beta = -\alpha$. The two boundary conditions are given by

$$\Phi = \Phi_o \text{ at } (x_o, 0) \text{ and } (-x_o, 0)$$

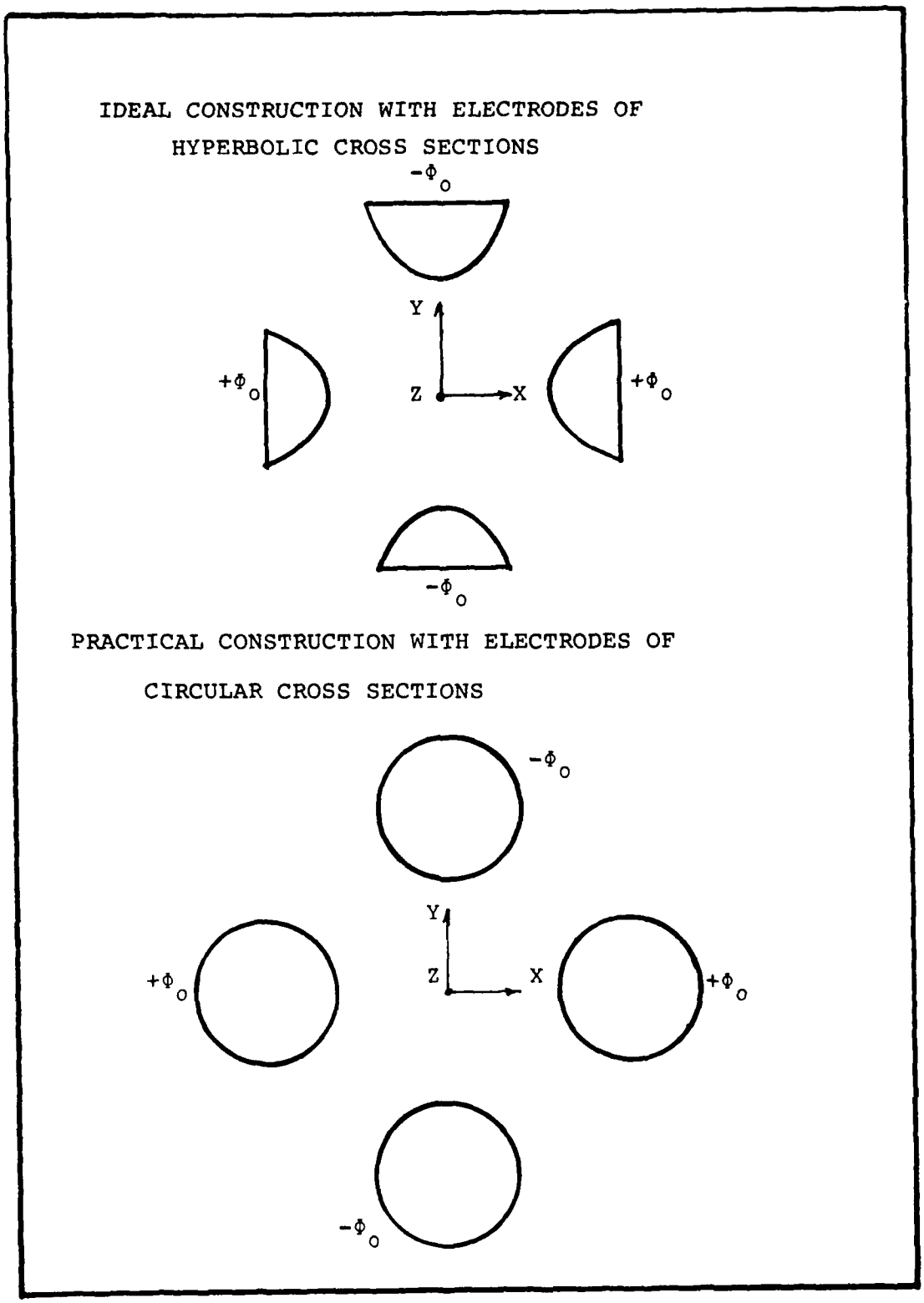

Figure 19. Electrode Configuration of the Electric Mass Filter

$$\Phi = -\Phi_o \text{ at } (0, y_o) \text{ and } (0, -y_o)$$

where x_o and y_o are the distances from the z-axis to the electrodes. Applying the two boundary conditions, $\alpha = \frac{1}{x_o^2}$ and $\frac{1}{y_o^2}$. Since the electrodes are in a square array, $x_o = y_o = r_o$ where r_o is the radius of the circle centered on the z-axis that is tangent to the surface of the electrodes. The final form of the potential is given by

$$\Phi = (U + V \cos \omega t) \frac{x^2 - y^2}{r_o^2} \qquad (B.2)$$

From Equation B.2, the equations of motion for a single charged ion are

$$m \ddot{x} + 2e (U + V \cos \omega t) \frac{x}{r_o^2} = 0 \qquad (B.3)$$

$$m \ddot{y} - 2e (U + V \cos \omega t) \frac{y}{r_o^2} = 0 \qquad (B.4)$$

$$m \ddot{z} = 0 \qquad (B.5)$$

The D.C. field has a focusing effect on the ions in the x- direction since $\ddot{x} \propto -Ux$ and a defocusing effect in the y- direction since $\ddot{y} \propto Uy$. The z-component of the velocity is constant.

Defining $\omega t = 2\rho$, Equations B.3 and B.4 are transformed into

$$\frac{d^2x}{d\rho^2} + (a + 2q \cos 2\rho)\, x = 0 \qquad (B.6)$$

$$\frac{d^2y}{d\rho^2} - (a + 2q \cos 2\rho)\, y = 0 \qquad (B.7)$$

where $a = \frac{8eU}{mr_o^2\omega^2}$ and $q = \frac{4eV}{mr_o^2\omega^2}$. Equations B.6 and B.7 are in the form

of Mathieu's differential equation. The solutions are stable if they tend to zero or remain bounded as ρ approaches $+\infty$ and unstable if they tend to $\pm\infty$ as ρ approaches $+\infty$. The stable solutions are known as the Mathieu and modified Mathieu functions, respectively; and the path of an ion is a high frequency oscillation about the z - axis. Ions that have stable trajectories are able to pass through the filter to the detector. The unstable solutions are exponential in nature, and the path of the ion diverges exponentially away from the z-axis until it eventually strikes an electrode and become neutralized. Stability depends on the choice of values for the dimensionless parameters a and q. For a detailed explanation of Mathieu functions and stability, see Reference 27.

Figure 20 shows the range of q-values corresponding to a certain a-value for which the solution is stable. An operating line is established by a constant a/q ratio, and this can be set by choosing the ratio U/V. If the operating line intersects the stability region (e.g., at points A and B in Figure 20), then there are (a,q) coordinate pairs on this line in the stability region that will produce a stable solution. Consequently, ions belonging to a certain e/m range have stable oscillations since a and q depend on e/m. As the operating line approaches the apex (point c) of the stability region, the e/m range becomes smaller, and the number of ions that are able to pass through the filter becomes less. When the operating line touches the apex, the e/m range is reduced to zero (infinite resolution) and there is a no transmission of ions.

The a and q values for infinite resolution are 0.237 and 0.706, respectively. Using the definitions of a and q, and assuming ions with a single charge,

$$U = 1.212\ M\ f^2\ r_o^2 \qquad (B.8)$$

$$V = 7.219\ M\ f^2\ r_o^2 \qquad (B.9)$$

where M is given in a m u, f in MHz, and r_o in cm. The numerical constants in Equations B.8 and B.9 are not unique, but depend on the

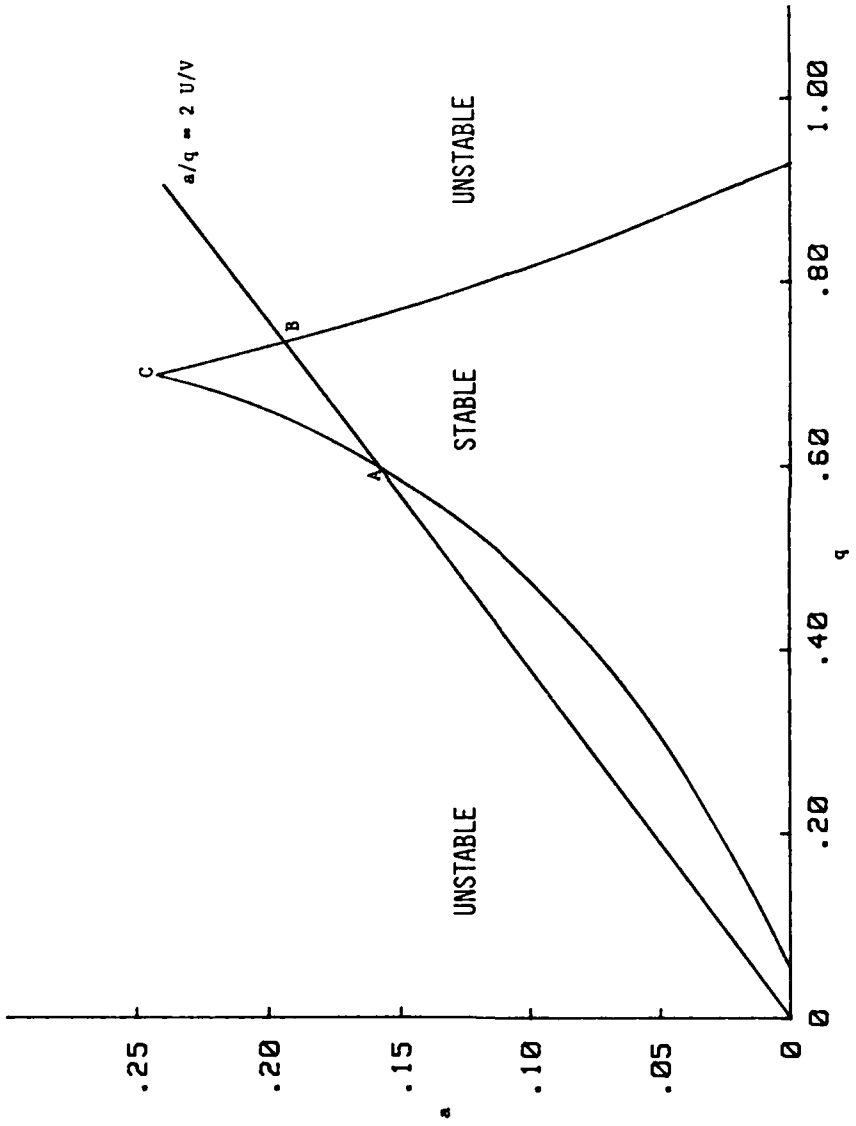

Figure 20. Stability Diagram of the Electric Mass Filter

values of a and q. The ratio U/V has a value of 0.16784 in the infinite resolution mode. Under normal operating conditions, therefore, the resolution can be adjusted by varying the two voltages, but the ratio U/V must be kept below 0.16784 for adequate transmission of ions. For high resolution, U and V must be chosen so that the operating line intersects the stability region near the apex.

For mass separation to occur, the ions of the incorrect e/m must remain in the filter long enough so that they will be rejected. Because of this requirement, the electrodes must be a minimum length for ions of a certain energy. If the ions are injected into the filter too far off from the z-axis, they will strike the electrodes even if they have the correct e/m. Hence, there is a restriction on the maximum distance from the z-axis that ions can be injected. The filter length and injection radius of the ions influence both the resolution and transmission (Reference 26).

From Equations B.8 and B.9, mass scanning can be accomplished by either varying U and V, or by varying f. If U and V are varied, they must be varied by the same amount in order to maintain a constant U/V ratio and, hence, constant resolution. All practical quadrupole power systems are designed so that U and V are varied while f is held constant. Also from Equations B.8 and B.9, the maximum mass range which can be scanned depends on f, U, V, and r_o. r_o can be varied by varying the diameter of the electrodes. The maximum values of U and V depend on the high power amplifier, and the maximum mass range depends only linearly with U and V. However, the maximum mass range depends on the square of f and r_o so that a large change in mass range requires only a minor change in the system's parameters f and r_o.

APPENDIX C

DATA REDUCTION

In order to arrive at a prediction of component concentrations, an expression for the total ion current density formed by the ionizer must be derived first. Figure 21 shows a schematic diagram of the axial ionizer most commonly used in an Extranuclear model EMBA II mass spectrometer. The neutral beam is admitted into a cylindrical grid which is surrounded by four filaments arranged in a square. Once inside, ions are produced by the interaction of neutral molecules with electrons of a certain energy formed by emission from the filaments and subsequent acceleration by the positive voltage on the grid.

The number of ionizing collisions per unit volume per unit time between electrons and molecules is given by (Reference 28):

$$\dot{n} = n_e \, n_s' < V\sigma_s (V) > \qquad (C.1)$$

where

n_e = the electron number density,

n_s' = the molecular number density of species s,

V = the magnitude of the relative velocity,

$\sigma_s (V)$ = the total ionization cross-section of molecular species s, which is a function of the relative velocity.

The $< \; >$ denotes a calculated average in velocity space of the product $V\sigma_s (V)$. The electrons possess most of the kinetic energy so that $V \simeq v_e$ where v_e is the speed of the electrons. This conclusion is justified as follows.

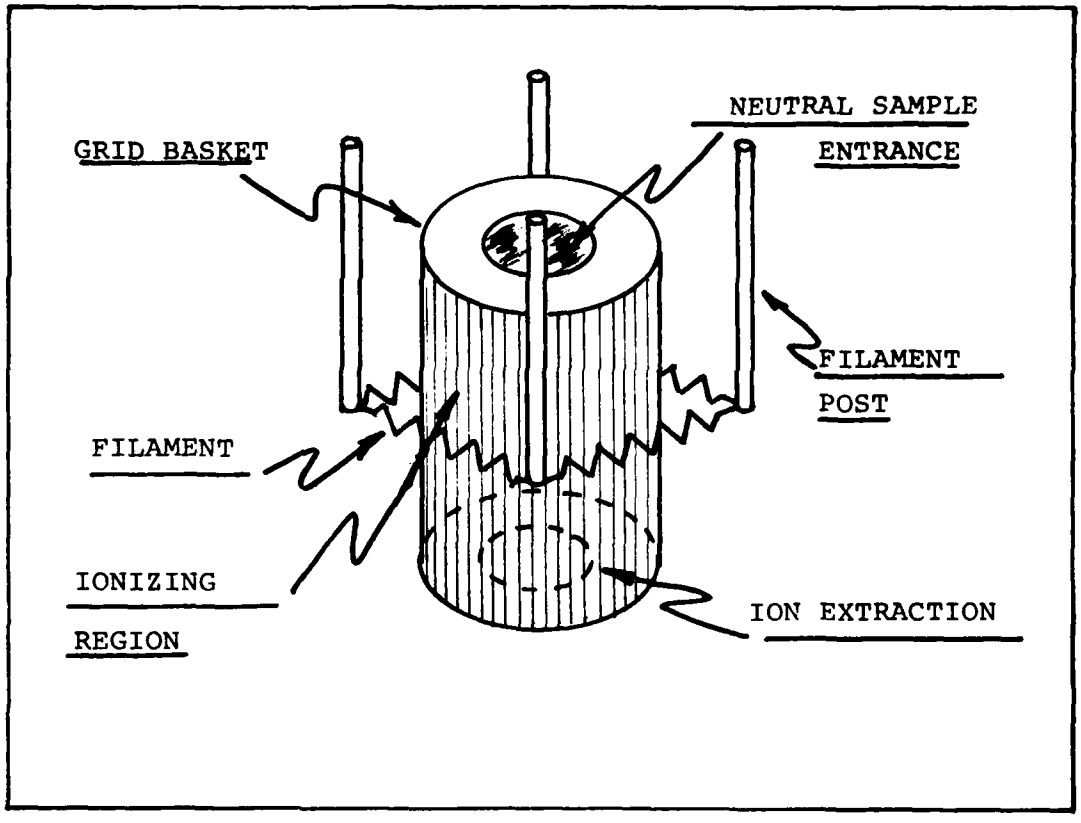

Figure 21. Axial Electron Impact Ionizer

For molecular flow, the average speed at which the molecules travel through the orifice is given by

$$\bar{v}_s = \left(\frac{8kT}{\pi m_s} \right)^{1/2} \qquad (C.2)$$

where T is the temperature of the source, m_s is the molecular mass, and k is Boltzmann's constant. This expression for the average speed assumes that the velocity distribution of the molecules in the source is Maxwellian. For a source containing Ar at 300°K, $\bar{v}_s \simeq 398$ m/sec. In a free jet expansion, the terminal speed of the molecules when they reach the ionizer is given by

$$v_s = \left[\left(\frac{2\gamma}{\gamma - 1} \right) \left(\frac{kT}{m_s} \right) \right]^{1/2} \qquad (C.3)$$

where γ is the ratio of the specific heat at constant pressure to the

specific heat at constant volume (Reference 29), and for an ideal monatomic gas $\gamma = 5/3$. Using the same Ar example, $v_s \simeq 558$ m/sec. From the examples above, the range of speeds are between 398 and 558 m/sec corresponding to the three types of flows: molecular, transition, and free jet expansion. The most common setting of the electron energy is 70eV for reasons explained in Section II. The speed of the electrons corresponding to this value of the energy is approximately 4.96×10^6 m/sec. Thus, the electron speed is approximately 890 times the speed of the molecules in a free jet expansion.

Replacing the magnitude of the relative velocity V with the speed of the electrons v_e, Equation C.1 reduces to

$$\dot{n} = n_e v_e n'_s \sigma_s \tag{C.4}$$

The number of ions formed per second in the ionizer is obtained by multiplying Equation C.4 by the volume of the interaction region. Hence,

$$\dot{N} = AL n_e v_e \sigma_s n'_s \tag{C.5}$$

where A is the cross sectional area of the entrance aperture to the grid and L is the length of the grid (see Figure 21). If these ions are now swept out as fast as they are produced, then the ion current density becomes

$$j_s = e n_e v_e L \sigma_s n'_s \tag{C.6}$$

In Equation C.6, the assumption has been made that the molecules are singly ionized. Also, the assumption has been made that the ionization process is not having to compete with other processes such as inelastic scattering, dissociation, etc. The product $en_e v_e$

is the electron current density; thus, Equation C.6 can further be reduced to

$$j_s = j_e L \sigma_s n_s' \tag{C.7}$$

For a detection system that has a linear response, the signal is proportional to the ion current density. Hence,

$$(PH)_s = C_s j_e L \sigma_s n_s' \tag{C.8}$$

where $(PH)_s$ is the "peak height" from the recorded mass spectrum and C_s is a constant of proportionality. The constant of proportionality is in general different for different species because they do not all give the same response when striking the multiplier.

The number density in the ionizer in terms of the number density in the source, in the case of molecular flow, is deduced as

$$n_s' = \frac{1}{4\pi D^2} A_o n_s \tag{C.9}$$

where n_s is the number density in the source, A_o is the cross sectional area of the sampling orifice, and D is the distance from the orifice to the ionizer (Reference 1). Substituting Equation C.9 into Equation C.8, the following result is obtained:

$$(PH)_s = (C_s j_e L A_o / 4\pi D^2)\, \sigma_s n_s \tag{C.10}$$

The spectrometer factor, F_s, is defined as $C_s j_e L A_o / 4\pi D^2$. Therefore,

$$(PH)_s = F_s \sigma_s n_s \tag{C.11}$$

The spectrometer factor depends on system parameters. It depends on the characteristics of the detection system through the constant of proportionality C_s. It depends on the characteristics and geometry

of the ionizer through the factors j_e and L, respectively. It also depends on the geometry of the sampling orifice through the quantity A_o and the geometry of the mass spectrometer through the quantity D.

The units of F_s depend on the units used for the peak height. If the peak height is read from a previously recorded mass spectrum the units are usually given in centimeters. Hence, the units of F_s are cm^2. On the other hand, if the peak height is recorded on a voltmeter connected to the electrometer or lock-in amplifier, the units are given in volts. Therefore, the units of F_s in this case are Vcm.

There are three primary requirements of gas analysis by mass spectrometry: (1) the peak height should be directly proportional to the number density of the gas sample in the source, (2) in a gas mixture, the sum of the peak heights should be a linear combination of the individual peak heights, and (3) the gas flow into the spectrometer should remain constant during a run. All of these requirements are satisfied in the molecular flow regime (Reference 1).

Comparing requirement (1) with Equation C.11, the product $F_s\sigma_s$ is a constant for any particular component. Figure 22 shows a plot of the peak height versus number density in the case of flowing the atomic gas Ar and the molecular gas N_2 individually through the discharge tube. The linearity of these curves are clearly evident, and the slopes of the lines are equal to $F_{Ar}\sigma_{Ar}$ and $F_{N_2}\sigma_{N_2}$ for Ar and N_2, respectively.

For a gas mixture, the spectrometer factor of a particular component will differ from the value it has in the case of individual gas flow through the discharge tube. This difference can be explained by considering requirement (2). In mathematical terms, requirement (2) can be expressed as

$$\sum_s (PH)_s = \sum_s k_s F_s \sigma_s n_s \qquad (C.12)$$

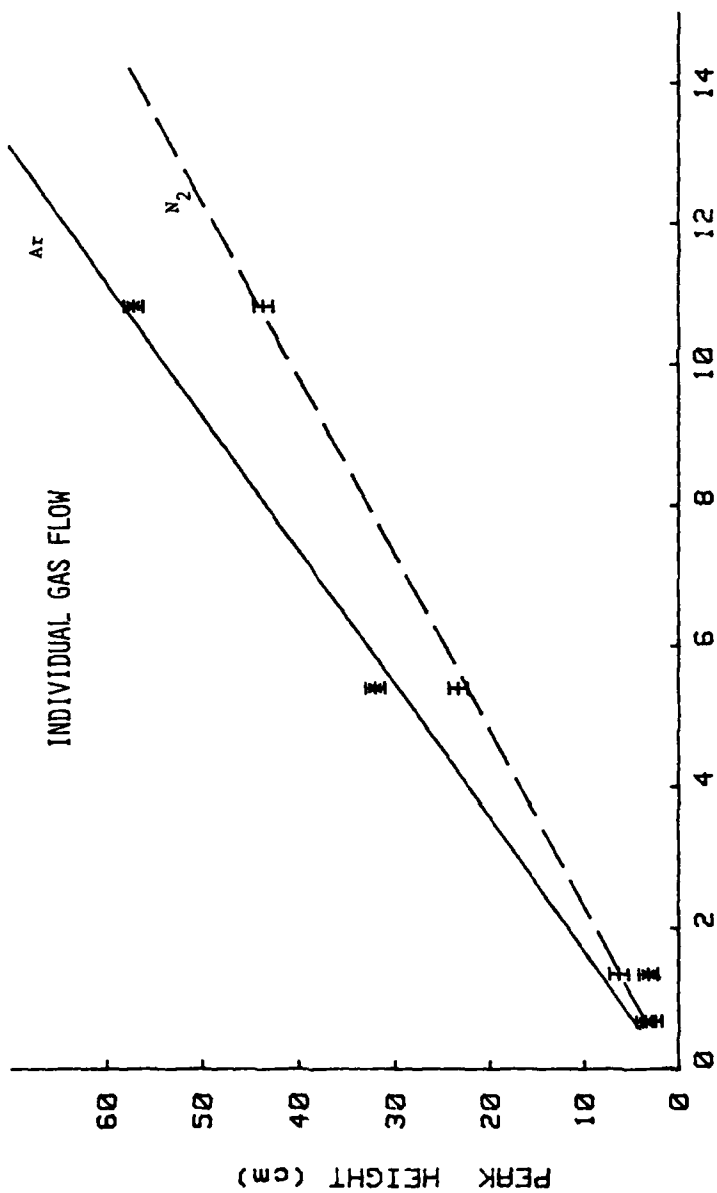

Figure 22. Signal Response in the Case of Individual Gas Flow

The signal contribution of a particular gas component is determined by tuning the mass filter to the mass number of the component. Equation C.12 then reduces to

$$(PH)_s = k_s F_s \sigma_s n_s = F_s' \sigma_s n_s \qquad (C.13)$$

where the coefficient k_s has been included in the spectrometer factor F_s'.

Figure 23 shows a plot of the peak height versus number density for Ar and N_2 in the case of an $Ar/N_2/CO_2/He$ mixture flowing through the discharge tube. Note the linearity below 15 X 10^{16} cm^{-3}; however, the slopes are different from the ones in Figure 22. At 27 X 10^{16} cm^{-3}, the deviation of the points from linearity is due to the fact that the total number density in the tube exceeded 10^{18} cm^{-3} and molecular flow was no longer valid for the size of orifice used. The diameter of the orifice was 2 mils in both individual and gas mixture flow.

In general, the spectrometer factors of the components in a gas mixture should be determined experimentally by using Equation C.13 and known number densities. This step must be done before the discharge is turned on. The factors are then used for normalizing component concentrations in the discharge. For new species produced in the discharge, an identification is made first; and then the spectrometer factors of these new components are determined by the method mentioned previously.

Under discharge conditions, there will be temperature and density variations in the tube due to gas heating. Therefore, the signal must be corrected in order to reflect the true signal (hence, true number density) in the absence of the effects of gas heating. There is a method for calculating the temperature rise and radial profiles in typical CO_2 laser mixtures (Reference 30). This method is somewhat laborious and requires the knowledge of specific parameters concerning

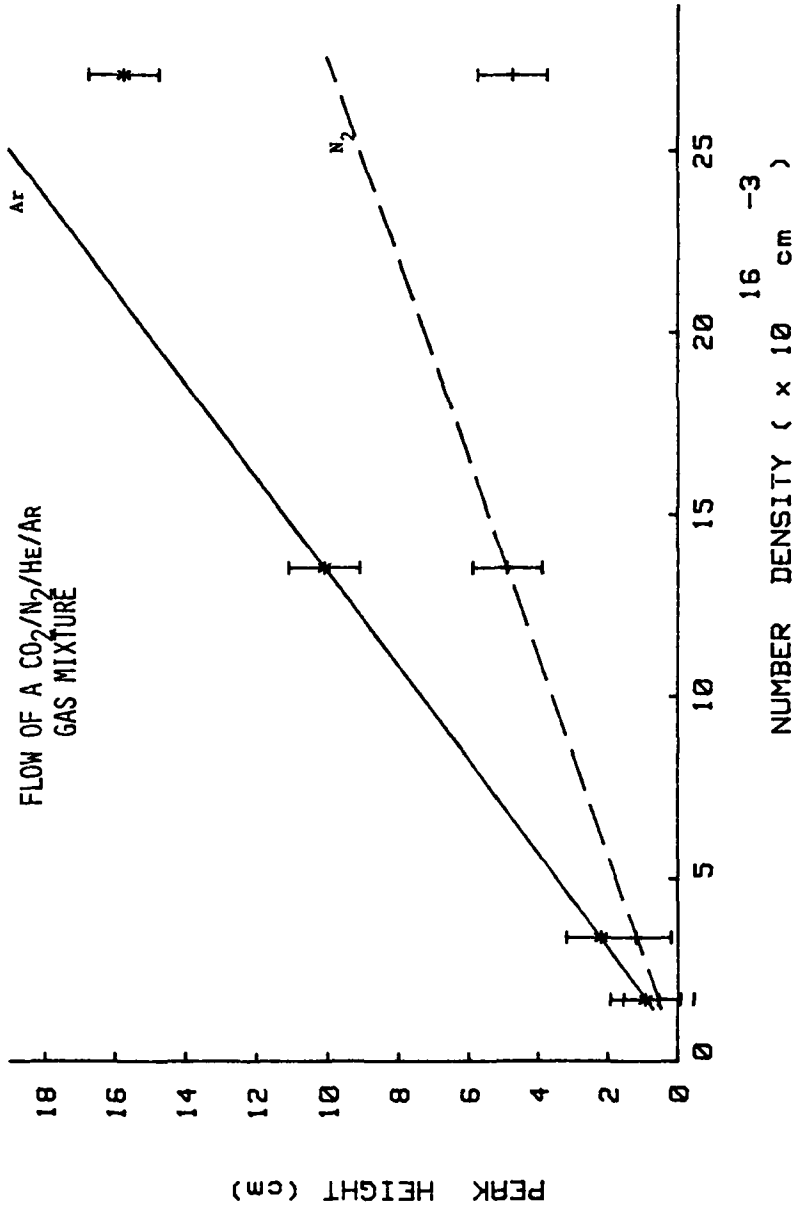

Figure 23. Signal Response in the Case of Gas Mixture Flow

the discharge. To monitor density changes due to gas heating, Ar is added to the mixture in question with a concentration less than or equal to 10%. Since Ar is inert, the change in its peak height is due to density variations alone. Hence, the peak height is corrected by multipling it by K_{Ar}, where K_{Ar} is defined as the ratio of the peak height with the discharge off to that of the peak height with the discharge on. K_{Ar} is also used to correct the other signals for the effects of gas heating. The assumption is that all gas components are heated uniformly throughout the volume. This assumption is not rigorously correct, but it represents a fair approximation.

It must be emphasized that the argon correction factor attempts to correct for the effects of gas heating alone. Pressure changes when the discharge is on may also be due to electrophoresis (References 31 and 32) as well as chemical dissociation.

REFERENCES

1. R.E. Honig, "Gas Flow in the Mass Spectrometer," Journal of Applied Physics, 16: pp. 646-654, (November 1945).

2. J.J. Sullivan and R.G. Buser, "Mass Spectrometric Sampling of Glow Discharges," J. Vac. Sci. Technol., 6: pp. 103-108, (1969).

3. P.D. Tannen, et al., "Species Composition In the CO_2 Discharge Laser," IEEE Journal of Quantum Electronics, QE-10: pp. 6-11, (January 1974).

4. R.J. Carbone, "Long-Term Operation of a Sealed CO_2 Laser," IEEE Journal of Quantum Electronics, QE-3: pp. 373-375, (September 1967).

5. R.G. Buser and J.J. Sullivan, "Initial Processes in CO_2 Glow Discharges," Journal of Applied Physics, 41: pp. 472-479, (February 1970).

6. N. Karube and E. Yamaka, "Mass-Spectrometric Studies of a Sealed CO_2 Laser," Journal of Applied Physics, 41: pp. 2031-2042, (April 1970).

7. A.L.S. Smith and J.M. Austin, "Dissociation Mechanism in Pulsed and Continuous CO_2 Lasers," J. Phys. D: Appl. Phys., 1: pp. 314-322, (1974).

8. K.K. Corvin and S.J.B. Corrigan, "Dissociation of Carbon Dioxide in the Positive Column of a Glow Discharge," The Journal of Chemical Physics, 50: pp. 2570-2574, (March 1969).

9. E.L. Gasilevich, et al., "Carbon Dioxide Dissociation in a CO_2 Laser," Soviet Physics-Technical Physics, 14: pp. 86-91, (July 1969).

10. W.J. Witteman, IEEE Journal of Quantum Electronics, QE-2: p. 375, (1966).

11. F.H.R. Almer, et al., "Influence of Hydrogen and Oxygen on the Gas Composition of Sealed-Off CO_2 Laser-Systems," Z. angen. Phys., 25: p. 166, (1968).

12. P. Bletzinger, et al., "Influence of Contaminants on the CO_2 Electric Discharge Laser," IEEE Journal of Quantum Electronics, QE-11: pp. 317-323, (July 1975).

13. P. Pace and M. Lacomb, "A Sealed High-Repetition-Rate TEA CO_2 Laser," IEEE Journal of Quantum Electronics, QE-14: pp. 263-274, (April 1978).

REFERENCES (Continued)

14. J.F. Prince, et al., "Carbon Monoxide Quenching of Negative Ions in the CO_2-N_2-He Electric Discharge Laser," Twenty-Eighth Annual Gaseous Electronics Conference, Rolla, MO., (October 1975).

15. J.F. Prince and A. Garscadden, "Negative Ion Species in $CO_2/N_2/He$ Discharges," Applied Physics Letters, 27: pp. 13-15, (July 1975).

16. J.M. Austin and A.L.S. Smith, "Analysis of Positive Ions in CO_2 Gas Laser Systems," J. Phys. D: Appl. Phys. 5: pp. 468-475, (1972).

17. F.R. Alger and F.A. Rees, "Positive and Negative Ion Reactions in Carbon Dioxide," J. Phys. D. Appl. Phys. 10: pp. 957-968, 1977.

18. P. Coxon and J.L. Moruzzi, "Ion-Molecule Reactions in CO_2 and CO_2-CO Mixtures," J. Phys. D: Appl. Phys., 10: pp. 967-977, (1977).

19. J. Sweemer and A. Garscadden, "Effects of Hydrogen in a Nitrogen-Carbon Dioxide Gas Discharge," Third Annual AIAA Mini-Symposium, Wright-Patterson AFB, Ohio: Air Force Institute of Technology, (March 1978).

20. M. Stamm, Air Force Institute of Technology (private communication).

21. A. Garscadden, Air Force Wright Aeronautical Laboratories (private communications).

22. D.E. Toodle, Synthesis of The Plasma Chemistry Occurring in High Power CO_2 Lasers, Master's thesis, Wright-Patterson AFB, Ohio Air Force Institute of Technology, (December 1978).

23. A. von Engel, Ionized Gases (Second Edition), London: Oxford University Press, (1965).

24. W. Paul and N. Steinwedel, Z. Naturforsch, 8a: p. 448, (1953).

25. W. Paul and M. Raether, Z. Physik, 140: p. 262, (1955).

26. W. Paul, et al., "The Electric Mass Filter as a Mass Spectrometer and Isotope Separator", Z. Physik, 151: pp. 143-182, (April 1958).

27. N.W. McLachlan, Theory and Application of Mathieu Functions. London: Oxford University Press, (1947).

28. C.V. Heer, Statistical Mechanics, Kinetic Theory, and Stochastic Processes. New York: Academic Press, (1972).

REFERENCES (Continued)

29. W.L. Fite, Expansion of Gases from Molecular Beam Sources, Research Note #1, Pittsburgh, Penn: Extranuclear Laboratories, Inc., (January 1971).

30. A.J. Laderman and S.R. Byrons, "Temperature Rise and Radial Profiles in CO_2 Lasers," Journal of Applied Physics, 42: pp. 3138-3144, (July 1971).

31. I. Langmuir, "The Pressure Effect And Other Phenomena In Gaseous Discharges," Journal of the Franklin Institute, 196: pp. 751-762, (December 1973).

32. M.J. Druyvesteyn, "The Electrophoresis In The Positive Column of a Gas Discharge," Physica, 1: pp. 255-266, (January 1935).

33. S.W. Benson, The Foundations of Chemical Kinetics. New York: McGraw-Hill, (1960).

34. W.J. Wiegand and W.L. Nighan, "Plasma Chemistry of $CO_2/N_2/He$ Discharges," Applied Physics Letters, 22: pp. 583-586, (January 1973).

35. H. Shields and A. Smith, "Negative Ion Effects in CO_2 Convection Laser Discharges," Appl. Phys., 16: pp 111-118 (1978).

36. H. Shields, et al., "Negative Ion Effects in TEA CO_2 Lasers," J. Phys. D: Appl. Phys., 9: pp. 1587-1603 (1976).

37. J. Thoenes and L. Kurzius, Plasma Chemistry Processes in Pulsed Electric Discharge Lasers, Technical Report RH-CR-76-12, Redstone Arsenal, Al.: U.S. Army Missile Command, (August 1976).

38. C.J. Elliot, et al., Electron Transport Coefficients and Vibrational Excitation Rates for Electrically Excited CO_2 Gas Lasers, Informal Report LA-5572-MS, Los Alamos, N.M.: Los Alamos Scientific Laboratory, (April 1974).

39 C. Cason, et al., A Small Scale Closed Cycle Circulator Experimental Plan For Repetitively Pulsed 200°K High Pressure Electric Discharge Lasers. Technical Report RH-76-12, Redstone Arsenal, Al.: U.S. Army Missile Command, (August 1976).

40. J.R. Action and J.D. Swift, Cold Cathode Discharge Tubes, New York: Academic Press, (1963).

REFERENCES (Concluded)

41. D.S. Jackson and H.I. Schiff, "Mass Spectrometric Investigation of Active Nitrogen," The Journal of Chemical Physics, 23: pp. 2333-2338 (December, 1955).

42. E.E. Ferguson, et al., "Flowing Afterglow Measurements of Ion-Neutral Reactions", Advances In Atomic And Molecular Physics, 5: pp. 1-56 (1969).

43. W. Bailey, Collision Induced Dissociation of Diatomic Molecules. Ph. D. Thesis. Wright-Patterson AFB, Ohio: Air Force Institute of Technology, (November 1978).

44. G. Herzberg, Spectra of Diatomic Molecules (Second Edition). New York: Van Nostrand Reinhold Company, (1950).

45. John Sweemer, United States Air Force (private communication).

46. W. Bailey, Air Force Institute of Technology (private communication).

BIBLIOGRAPHY

The following bibliography represents general references on the subject of mass spectrometry and mass spectrometric sampling.

Cuthber, J. "Mass Spectrometric Sampling And Detection Of Intermediates In Gaseous Reactions," in Advances In Mass Spectrometry, Vol. 3, edited by W.L. Mead London: The Institute of Petroleum, (1966).

Drawin, H.W. "Mass Spectrometry Of Plasmas," in Plasma Diagnostics, edited by W. Lochte-Holtgreven Amsterdam: North-Holland Publishing Company, (1968).

Greene, F.T. and Milne, T.A. "Mass Spectrometric Sampling Of High Pressure-High Temperature Sources," in Advances In Mass Spectrometry, Vol. 3, edited by W.L. Mead, London: The Institute of Petroleum, (1966).

Helm, H. et al., "A Quantitative Analysis Of Ion-Molecule Reactions Occurring Within The Extraction Orifice Of A Mass-Spectrometric Sampling Probe," J. Phys. B: Atomic and Molecular Physics, 7: pp. 170-177 (1974).

Kinsman, P.R. and Rees, J.A. "A Method Of Evaluating Mass Discrimination Effects In The Mass Spectrometry Of Ions From High Pressure Electrical Discharges," J. Phys. E: Scientific Instruments, 3: pp. 444-446. (1970).

Knewstubb, P.F. and Tickner, A.W. "Mass Spectrometry Of Ions In Glow Discharges. I. Apparatus and Its Application to the Positive Column in Rare Gases," The Journal Of Chemical Physics, 36: pp. 674-683 (1962).

Robertson, A.J.B., Mass Spectrometry, New York: Wiley, (1954).

Roboz, J. Introduction To Mass Spectrometry: Instrumentation And Techniques, New York: Interscience Publishers, (1968).

BIBLIOGRAPHY (Concluded)

Smith, D. and Plumb, I.C., "An Appraisal of the Mass Spectrometer Diagnostic Technique in the Study of Afterglow Plasmas," J. Phys. D: Appl. Phys., 6: pp. 1431-1446 (1973).

Stearns, C.A. et al., High Pressure Molecular Beam Mass Spectrometric Sampling Of High Temperature Molecules, Proceedings of the 10th Materials Research Symposium on Characterization of High Temperature Vapors and Gases, Gaithersburg, Maryland: National Bureau of Standards, (September 1978).

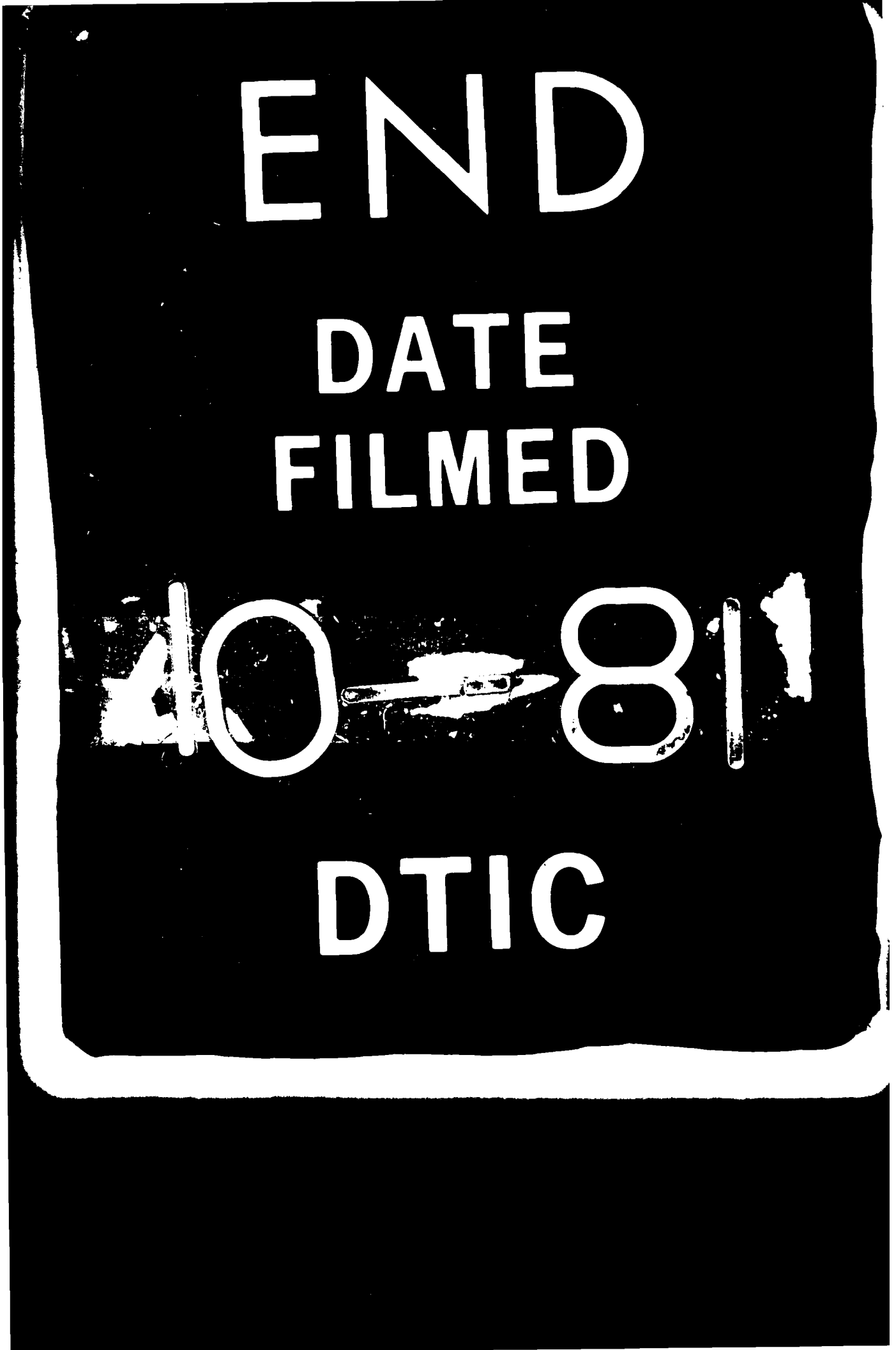
END
DATE
FILMED
10-81
DTIC